cmgh
CELLULAR AND MOLECULAR GASTROENTEROLOGY AND HEPATOLOGY

ORIGINAL RESEARCH

Unique T-Cell Populations Define Immune-Inflamed Hepatocellular Carcinoma

Daniela Di Blasi,[1,2] Tujana Boldanova,[2,3] Lucia Mori,[1] Luigi Terracciano,[4] Markus H. Heim,[2,3,§] and Gennaro De Libero[1,§]

[1]Experimental Immunology, [2]Hepatology Laboratory, Department of Biomedicine, University of Basel, Switzerland; [3]Division of Gastroenterology and Hepatology, [4]Institute of Pathology, Division of Molecular Pathology, University Hospital Basel, Basel, Switzerland

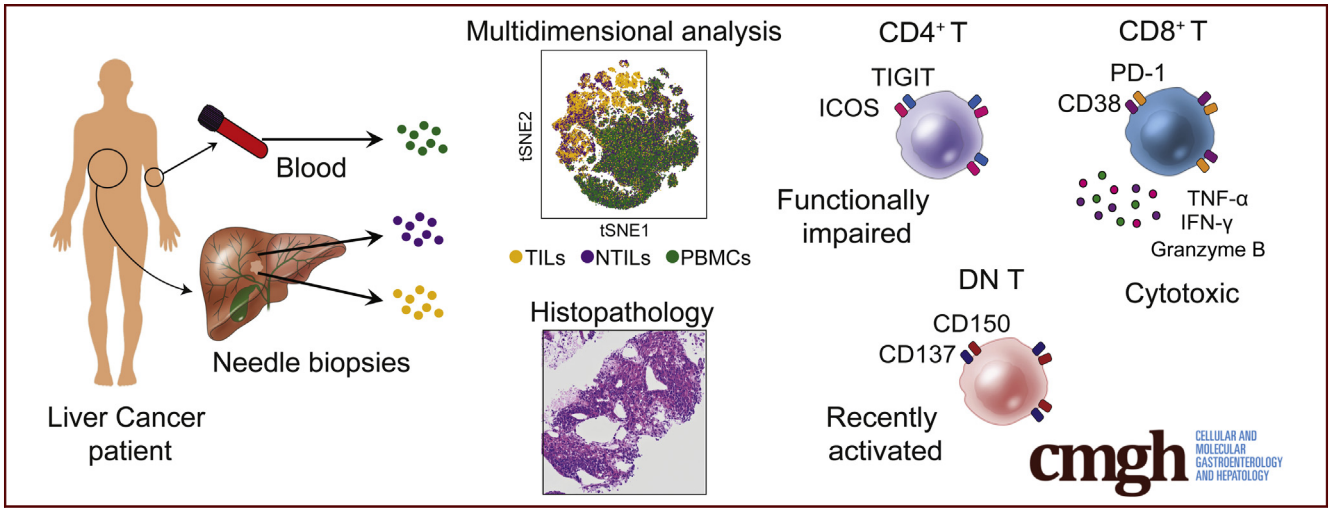

SUMMARY

Immune profiling of hepatocellular carcinoma–infiltrating cells showed unique T-cell populations, including impaired ICOS$^+$, TIGIT$^+$, CD4$^+$ T cells, activated CD8$^+$, and non–major histocompatibility complex restricted T cells. Immunotherapy with check-point inhibitors diminished nonfunctional T cells and increased the number of responding cells.

BACKGROUND & AIMS: The characterization of T cells infiltrating hepatocellular carcinoma (HCC) provides information on cancer immunity and also on selection of patients with precise indication of immunotherapy. The aim of the study was to characterize T-cell populations within tumor tissue and compare them with non-neoplastic liver tissue as well as circulating cells of the same patients.

METHODS: The presence of unique cell populations was investigated in 36 HCC patients by multidimensional flow cytometry followed by t-distributed stochastic neighbor embedding analysis. Functional activity of tumor-infiltrating T cells was determined after activation by phorbol 12-myristate 13-acetate and ionomycin.

RESULTS: Within the tumor there were more cells expressing CD137 and ICOS than in non-neoplastic liver tissue, possibly after recent antigenic activation. These cells contained several populations, including the following: (1) functionally impaired, proliferating CD4$^+$ cells co-expressing Inducible T-cell costimulator (ICOS) and T cell immunoreceptor with Ig and ITIM domains (TIGIT); (2) functionally active CD8$^+$ cells co-expressing CD38 and Programmed cell-death protein 1 (PD1); and (3) CD4-CD8 double-negative T-cell receptor $\alpha\beta$ and $\gamma\delta$ cells (both non–major histocompatibility complex–restricted T cells). When the identified clusters were compared with histologic classification performed on the same samples, an accumulation of activated T cells was observed in immune-inflamed HCC. The same analyses performed in 7 patients receiving nivolumab treatment showed a remarkable reduction in the functionally impaired CD4$^+$ cells, which returned to almost normal activity over time.

CONCLUSIONS: Unique populations of activated T cells are present in HCC tissue, whose antigen specificity remains to be investigated. Some of these cell populations are functionally impaired and nivolumab treatment restores their responsiveness. The finding of ongoing immune response within the tumor shows which lymphocyte populations are impaired within the HCC and identifies the patients who might take benefit from immunotherapy. *(Cell Mol Gastroenterol Hepatol 2020;9:195–218; https://doi.org/10.1016/j.jcmgh.2019.08.004)*

Keywords: Cancer Immunity; Immunotherapy; tSNE Analysis.

Hepatocellular carcinoma (HCC) is the second leading cause of worldwide mortality[1] and is the most common primary liver cancer, accounting for 90% of all liver cancers.[2] Epidemiologic studies have shown that HCC occurs mostly in patients with chronic liver diseases including those caused by hepatitis viral infection, alcohol abuse, nonalcoholic steatohepatitis, obesity, and exposure to the fungal aflatoxin B1 toxin.[2,3]

Inflammation can be an essential component of cancer development and also facilitates cell growth.[4] In HCC, the chronic liver inflammation is sustained by activation of innate and adaptive immune cells that contribute to liver damage, leading to cell transformation and tumor cell invasion of liver tissue.[5] Immune cells accumulating within the tumor also may exert antitumor activities, thereby their characterization may acquire an important prognostic value.[6] Indeed, a recently proposed classification of tumors was based on the presence of lymphocytic infiltrate in the tumor microenvironment[6]: inflamed tumors are those with lymphocytic infiltrate; immune-excluded, those with lymphocytes only at tumor edges, and immune-desert, those with minimal numbers of lymphocytes near tumor tissue. Inflamed tumors usually are characterized by local production of proinflammatory cytokines and are associated with a high response rate to anticheckpoint therapy.[6] However, which tumor-infiltrating lymphocytes correlate with antitumor response, or are unleashed by anticheckpoint therapy, remains unclear. Importantly, it also is unknown whether unique lymphocytes that are present in inflamed tumors are predictive of therapy response and have prognostic value.

Tumor-infiltrating lymphocytes (TILs) have been studied for their prognostic value in several human tumors,[7,8] including HCC,[9] in which the presence of T cells and the absence of macrophages correlated with patient survival. These studies did not show whether unique T-cell populations preferentially infiltrate HCC.

It also remains unknown whether HCC TILs are functionally impaired and, if so, which population then becomes the antigen-nonresponder. Unresponsive T cells might represent tumor-specific lymphocytes, which are potential targets of immunomodulatory therapies. Current HCC treatment options remain unsatisfactory. The use of the immune checkpoint inhibitor nivolumab in HCC patients lead to durable objective responses, although in a small percentage of patients.[10] The small efficacy might be a consequence of expression of other inhibitory receptors by HCC TILs. Therefore, the identification of the populations providing antitumor immunity might be of great help to define personalized checkpoint inhibitory therapy and increase the chance of therapy response.

In this study we performed a multidimensional analysis of TILs infiltrating HCC and compared them with T cells present in nontumor liver (non–tumor infiltrating lymphocytes [NTILs]) and peripheral blood mononuclear cells (PBMCs) of the same donors. Within HCC we found evidence of recently activated $CD4^+$, $CD8^+$, and CD4-CD8 double-negative (DN) unique T-cell populations. Some of these cells were exhausted effector T cells that recovered immune responsiveness upon nivolumab treatment. These phenotypic and functional characteristics of HCC TILs identify novel T-cell populations that might be the target of immunotherapy in this type of tumor.

Results

Patient and Biopsy Cohort

A total of 36 patients were studied and their clinical and pathologic characteristics are summarized in Table 1. HCC biopsy specimens were obtained from 34 patients before therapeutic treatment. Eleven HCC biopsy specimens were obtained from 7 nivolumab-treated (anti-PD1 immunotherapy) patients. The patients were predominantly male (83.3%), and half of them (47.2%) suffered from cirrhosis. From each HCC patient paired samples of peripheral blood and nontumor liver biopsy specimens also were obtained.

$CD4^+$ T Cells Are Enriched in Tumor Tissue

Comparative analyses were performed on samples obtained from TILs, NTILs, and PBMCs. The frequency of $CD4^+$ T cells in TILs was significantly higher compared with NTILs (66.6% ± 3.36% vs 45.25% ± 2.9% of $CD3^+$ T cells; $P = .0001$). On the contrary, $CD8^+$ and DN T-cell frequencies were lower in TILs compared with NTILs (25.3% ± 3.41 vs 40.8% ± 2.77 for $CD8^+$ T cells; $P = .02$; and 4.44% ± 1 vs 7.24% ± 1.7 for DN T cells; $P = .0018$). Within the DN T cells, T-cell receptor (TCR) $\gamma\delta$ cells were reduced in the tumor compared with nontumor liver (2.85% ± 1.53 vs 7.15% ± 1.71; $P = .01$), whereas mucosal-associated invariant T (MAIT) cells did not show major differences in TILs vs NTILs (2.57% ± 0.8 vs 3.28% ± 0.96, respectively) (Figure 1*A*). The percentages of $CD4^+$, $CD8^+$, DN, and TCR $\gamma\delta$ T cells were not different between TILs and PBMCs. The frequencies of MAIT cells in TILs and NTILs were higher than in the PBMCs (2.13% ± 0.5 and 0.73% ± 0.22, respectively; $P = .0007$), confirming the preferential localization of MAIT cells into the liver.[11,12] Taken together, these data showed that $CD4^+$ T cells are enriched whereas $CD8^+$, DN, and TCR $\gamma\delta$ T cells are decreased in HCC compared with nontumor liver.

[§]Authors share co-senior authorship.

Abbreviations used in this paper: **DBSCAN, density-based spatial clustering application with noise algorithm; DN, CD4-CD8 double-negative; HCC, hepatocellular carcinoma; IFN, interferon; IL, interleukin; MAIT, mucosal-associated invariant T cell; NTIL, nontumor liver-infiltrating lymphocyte; PBMC, peripheral blood mononuclear cell; PBS, phosphate-buffered saline; PMA, phorbol 12-myristate 13-acetate; TCR, T-cell receptor; TIL, tumor-infiltrating lymphocyte; TNF, tumor necrosis factor; Treg, regulatory T cell; tSNE, t-distributed stochastic neighbor embedding.**

Most current article

2352-345X
https://doi.org/10.1016/j.jcmgh.2019.08.004

Table 1. Clinical and Pathologic Characteristics of HCC Patients

Patient	Tumor biopsy code	Cell number, 10^6	Edmondson–Steiner grade, I–IV	TIM	Intratumoral TIL, %	Stroma TIL, %	Time point	Sex	YOB	BCLC	Cirrhosis	Liver Disease	AFP
1	D403	4.5	II	3	0	0	Pretreatment	M	1944	A	No	NAFLD	9.5
2	D214	20	II	2	0	30	Pretreatment	M	1944	A	Yes	ALD	7.2
3	D316	3.5	II	3	0	0	Pretreatment	M	1932	A	No	NAFLD	1
4	D373	7.5	II	2	5	30	Pretreatment	F	1938	A	No	HEP C	5.6
4	D557	2.5	III	1	20	20	Nivolumab	F	1938	A	No	HEP C	5.6
5	D143	2	III	1	20	20	Pretreatment	F	1954	D	Yes	ALD	6
6	D330	30	II	1	10	20	Pretreatment	M	1938	C	Yes	ALD	48
6	D448	1.4	II	1	10	30	Nivolumab	M	1938	C	Yes	ALD	48
7	D096	3.5	IV	1	20	20	Pretreatment	M	1941	A	No	ALD	2
8	D324	10	III	1	10	20	Pretreatment	M	1959	D	Yes	ALD	104,710
9	D332	3.6	II	1	10	20	Pretreatment	M	1945	A	No	ALD	3.1
10	D359	18	III	1	20	NA	Pretreatment	M	1930	B	No	ALD and NAFLD	5917
11	D147	4.5	III	1	10	10	Pretreatment	M	1948	A	No	HEP B	32.5
12	D562	2.5	II	2	5	30	Pretreatment	M	1943	A	Yes	HEP C	2.5
13	D304	NA	III	3	5	0	Pretreatment	M	1953	A	No	HEP C and ALD	NA
14	D588	2.5	II	3	0	0	Pretreatment	M	1932	A	No	NAFLD	338
15	D565	5	IV	1	20	5	Pretreatment	M	1974	C	No	NAFLD	645
16	D274	1.6	III	1	10	10	Pretreatment	M	1936	A	Yes	NAFLD	1.3
17	D029	2	II	2	0	40	Pretreatment	F	1943	B	Yes	ALD	7.9
18	D113	0.8	III	1	10	30	Pretreatment	M	1937	A	No	ALD and NAFLD	49.8
18	D386	6	III	1	30	20	Pretreatment	M	1937	A	No	ALD and NAFLD	49.8
18	D388	1.2	III	1	30	20	Pretreatment	M	1937	A	No	ALD and NAFLD	49.8
19	D336	18	II	3	5	0	Pretreatment	M	1936	C	Yes	ALD	6.6
19	D572	2	II	1	10	10	Nivolumab	M	1936	C	Yes	ALD	6.6
19	D573	2.5	II	3	0	0	Nivolumab	M	1936	C	Yes	ALD	6.6
20	D268	30	II	1	20	NA	Pretreatment	M	1946	B	Yes	ALD and NAFLD	10.2
21	D240	60	II	3	5	5	Pretreatment	M	1944	B	Yes	ALD and NAFLD	5.6
22	D228	60	II	1	10	20	Pretreatment	M	1936	A	Yes	ALD	3.6
23	D483	1.2	II	1	20	20	Pretreatment	M	1934	A	No	ALD and NAFLD	2.7
24	D176	40	II	3	0	0	Pretreatment	M	1937	C	No	NAFLD	0.9
25	D020	NA	III	1	30	5	Pretreatment	F	1945	C	Yes	ALD	1745
26	D302	150	III	1	30	20	Pretreatment	F	1949	C	Yes	ALD	400,000
27	D158	18	II	2	0	30	Pretreatment	F	1939	B	Yes	NAFLD	4.6
28	D156	60	II	NA	5	NA	Pretreatment	M	1949	A	Yes	HEP B	2

Table 1. Continued

Patient	Tumor biopsy code	Cell number, 10^6	Edmondson–Steiner grade, I–IV	TIM	Intratumoral TIL, %	Stroma TIL, %	Time point	Sex	YOB	BCLC	Cirrhosis	Liver Disease	AFP
29	D017	NA	III	NA	5	NA	Pretreatment	M	1933	A	No	ALD	231
30	D045	1.5	III	3	0	5	Pretreatment	M	1947	A	Yes	HEP C	7852
31	D135	1.9	IV	1	10	30	Pretreatment	M	1959	C	Yes	HEP C	11.4
32	D200	21	II	3	0	0	Pretreatment	M	1940	B	No	ALD and NAFLD	1615
32	D201	30	III	1	20	NA	Pretreatment	M	1940	B	No	ALD and NAFLD	1615
32	D202	20	II	3	0	NA	Pretreatment	M	1940	B	No	ALD and NAFLD	1615
32	D318	4	II	3	0	5	Pretreatment	M	1940	B	No	ALD and NAFLD	1615
32	D319	2.7	II	3	0	0	Pretreatment	M	1940	B	No	ALD and NAFLD	1615
32	D505	NA	III	NA	0	NA	Nivolumab	M	1940	B	No	ALD and NAFLD	1615
33	D503	NA	III	1	20	20	Pretreatment	M	1941	B	No	NASH	3995
34	C948	NA	III	1	20	20	Pretreatment	M	1958	C	Yes	HEP C and ALD	12,054
34	C949	NA	III	1	30	30	Pretreatment	M	1958	C	Yes	HEP C and ALD	12,054
34	D001	1.7	III	1	30	30	Nivolumab	M	1958	C	Yes	HEP C and ALD	12,054
35	D470	NA	III	1	20	10	Nivolumab	M	1958	C	No	HEP C and NASH	3.9
36	D152	60	II	1	20	0	Nivolumab	M	1943	B	No	HEP C	1057
36	D153	60	I	2	5	10	Nivolumab	M	1943	B	No	HEP C	1057
36	D340	6	II	1	20	0	Nivolumab	M	1943	B	No	HEP C	1057
36	D341	7	I	2	0	10	Nivolumab	M	1943	B	No	HEP C	1057

NOTE. For the tumor-immune microenvironment, 1 indicates immune-inflamed, 2 indicates immune-excluded, and 3 indicates immune-desert.
AFP, α-fetoprotein; ALD, alcoholic liver disease; BCLC, Barcelona Clinic Liver Cancer; HEP B, hepatitis B; HEP C, hepatitis C; NA, not applicable; NAFLD, nonalcoholic fatty liver disease; NASH, nonalcoholic steatohepatitis; TIM, tumor-immune microenvironment; YOB, year of birth.

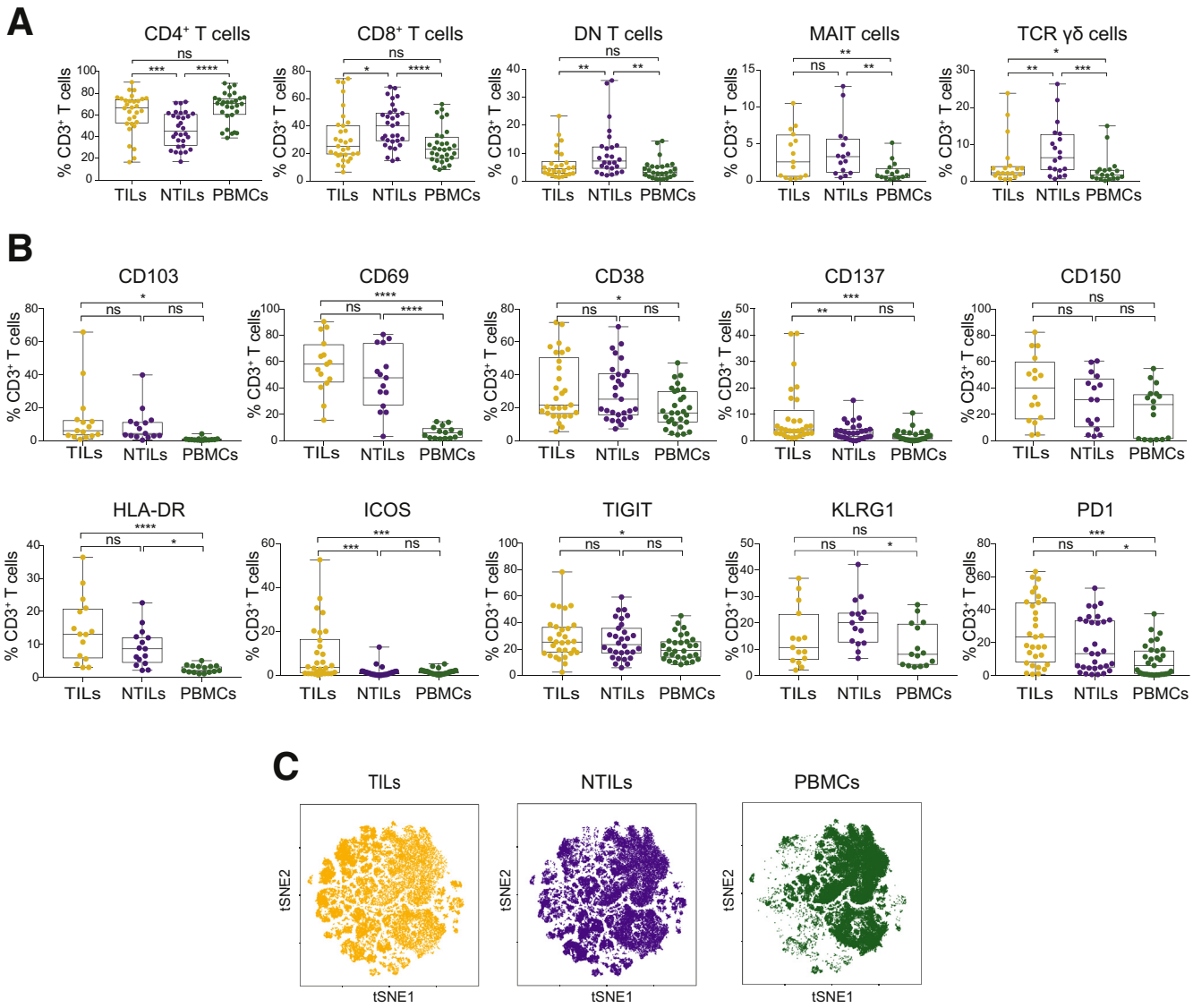

Figure 1. Frequency and phenotype of CD3$^+$ T-cell subsets in HCC patients. (*A*) Box plots showing the frequency of CD4, CD8, DN, MAIT, and TCR $\gamma\delta$ cells in TILs vs NTILs and PBMCs. Each *dot* represents an individual sample. (*B*) *Box plots* showing the phenotype of CD3$^+$ cells. The percentage of cells expressing the indicated markers is indicated for each sample. (*C*) tSNE map of total CD3$^+$ cells in TILs (*yellow dots*), NTILs (*purple dots*), and PBMCs (*green dots*). *$P \leq .05$, **$P \leq .01$, ***$P \leq .001$, and ****$P \leq .0001$, 2-tailed paired test for multiple comparison (Tukey test). ns, not significant.

The underlying liver disease (viral hepatitis vs alcoholic hepatitis) did not show direct influence on the immune infiltrate, with the exception of a slightly larger number of CD4 cells in NTILs and PBMCs (Figure 2).

CD137 and ICOS Expressing T Cells Are Enriched in the Tumor

Next, a multiparametric flow cytometry analysis was performed to characterize TIL phenotype and functional state. The expression of activation markers (CD103, CD69, CD38, CD137, CD150, HLA-DR, and ICOS) and inhibitory receptors (TIGIT, KLRG-1, and PD1) was compared on T cells isolated from TILs, NTILs, and PBMC (see list of analyzed molecules in Table 2). Increased expression of CD137 and ICOS were found on TILs vs NTILs ($P = .005$ and $P = .0002$, respectively) and vs PBMCs ($P = .0001$ and $P = .0001$, respectively) (Figure 1*B*). Of note, these markers were similarly expressed by NTILs and PBMCs, indicating that their expression was tumor-associated and not a consequence of liver homing. The increased CD137 and ICOS expression indicated the presence of recently activated T cells in the tumor.[13] To assess whether these markers might show the emergence of unique T cells infiltrating HCC tissue, we analyzed all markers using the t-distributed stochastic neighbor embedding (tSNE) algorithm that reduces all data to 2 dimensions (Figure 1*C*). Unique populations appeared in TILs whereas the major cell clusters in NTILs and PBMCs were very similar to each other. NTILs also showed small clusters different from PBMCs, which probably reflect unique liver-resident T-cell populations.

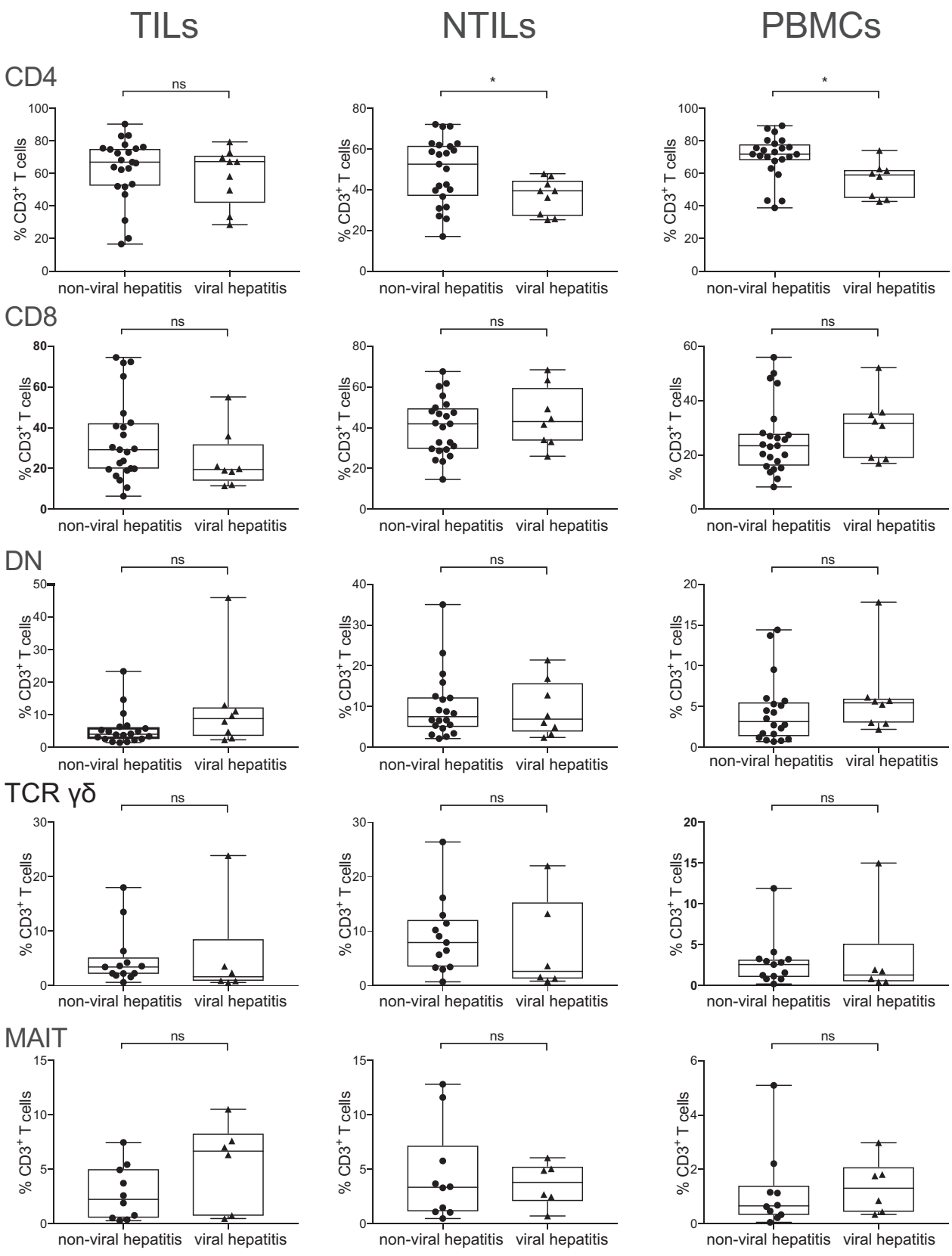

Figure 2. Frequency and phenotype of CD3$^+$ T-cell subsets in viral and nonviral hepatitis. *Box plots* showing the frequency of CD4, CD8, DN, MAIT, and TCR $\gamma\delta$ cells in TILs, NTILs, and PBMCs. Each *dot* represents an individual sample. *$P \leq$ .05, Wilcoxon signed-rank test, adjusted with the Benjamini and Hochberg method. ns, not significant.

Table 2. Cell Surface Immunostaining Panel 1

Marker	Dye	Host species	Reactivity	Clone	Description	Catalog no
CD3	PE/Cy7	Mouse	Human	UCHT1	Co-receptor: CD3 T cells	300420
CD4	Brilliant Violet 711	Mouse	Human	OKT4	Co-receptor: CD4 T cells	317440
CD8	BUV 496	Mouse	Human	RPA-T8	Co-receptor: CD8 T cells	564804
TCR $\gamma\delta$	Brilliant Violet 421	Mouse	Human	B1	T-cell receptor: TCR $\gamma\delta$	331218
hMR1-5OP-RU Tetramer	PE		Human		MR1-Ag tetramer: MAIT cells	31704 R
CD19	PE/Cy5	Mouse	Human	J3-119	Co-receptor: B cells	A07771
CD14	PE/Cy5	Mouse	Human	RMO52	Co-receptor: monocytes	A07765
CD137	PE/Dazzle 594	Mouse	Human	4B4-1	Costimulatory receptor	309826
CD278 (ICOS)	Brilliant Violet 510	Mouse	Human	C398.4A	Costimulatory receptor	313525
CD150 (SLAM)	FITC	Mouse	Human	A12 (7D4)	Costimulatory receptor	306306
CD38	Brilliant Violet 650	Mouse	Human	HB-7	cADP ribose hydrolase	356620
HLA-DR	Alexa Fluor 700	Mouse	Human	L243	Ag presenting molecule	307626
CD69	APC/Cy7	Mouse	Human	FN50	Adhesion molecule	310914
CD103	APC	Mouse	Human	Ber-ACT8	Adhesion molecule	350216
TIGIT (VSTM3)	PerCP-eFluor 710	Mouse	Human	MBSA43	Inhibitory receptor	46-9500-42
PD1	Brilliant Violet 785	Mouse	Human	EH12.2H7	Inhibitory receptor	329930
KLRG1	Brilliant Violet 605	Mouse	Human	2F1/KLRG1	Inhibitory receptor	138419

Ag, antigen; cADP, cyclic adenosine diphosphate; FITC, fluorescein isothiocyanate; PE, phycoerythrin.

These data clearly indicated that HCC TILs are different form liver-resident T cells and might have immunologic relevance.

Enrichment of ICOS$^+$ TIGIT$^+$ CD4$^+$ T Cells in HCC Vs Nontumor Liver and Peripheral Blood

To better characterize HCC-associated clusters, tSNE analysis was performed on individual CD4$^+$, CD8$^+$, and DN T-cell subpopulations. The distribution of CD4$^+$ T cells in tumor liver (yellow), in nontumor liver (purple), and in PBMCs (green) from 15 HCC patients is shown in Figure 3*A*. High expression of multiple activation markers (CD69, ICOS, CD150, CD137, HLA-DR, and ICOS) and inhibitory receptors (PD1 and TIGIT) mostly contributed to different clustering of CD4$^+$ TILs (Figure 3*B*). As expected, small numbers of MAIT and TCR $\gamma\delta$ cells were present in the CD4$^+$ compartment and did not show significant differences between TILs and NTILs. Further analyses of CD4$^+$ T cells performed using the density-based spatial clustering application with noise algorithm (DBSCAN) algorithm[14] showed 11 clusters (CD4-1, -2, -3, -4, -5, -7, -8, -10, -11, -14, and -19) significantly enriched in HCC vs NTILs and PBMCs (Figure 3*C* and *D*). These clusters shared high levels of TIGIT and ICOS and differed in the expression of other activation markers and inhibitory receptors (Figure 3*E*). All clusters, except cluster CD4-1, CD4-2, and CD4-19, expressed high levels of CD137, a marker associated with recent T-cell activation.[13] Furthermore, most CD137$^+$ activated cells also expressed PD1, probably indicating that these cells had undergone multiple rounds of activation within HCC.[15,16] The expression of CD69 suggested that they were tissue-resident cells within the tumor,[17] although this marker also may indicate previous antigen stimulation. Collectively, these data showed that CD4$^+$ T cells co-expressing ICOS and TIGIT were preferentially accumulated in the tumor compared with the nontumor liver and PBMCs.

ICOS$^+$ TIGIT$^+$ CD4$^+$ TILs Proliferate in HCC But Are Functionally Impaired

The effector functions of CD4$^+$ and CD8$^+$ HCC TILs, were investigated in a second cohort of patients that also served as validation of the first HCC cohort. Matched TILs, NTILs, and PBMCs of 13 HCC patients were stimulated with phorbol 12-myristate 13-acetate (PMA) and ionomycin and analyzed by 13-parameter flow cytometry for their expression of activation markers and effector molecules (see list of analyzed molecules in Table 3). The analysis of interferon-γ (IFN-γ), tumor necrosis factor-α (TNF-α), interleukin (IL)22, granzyme B, and perforin showed 19 clusters in CD4$^+$ T cells (Figure 4*A* and *B*). These results also confirmed that in this second cohort of patients, ICOS$^+$ CD137$^+$ TIGIT$^+$ PD1$^+$ T cells (cluster CD4-6) were enriched in HCC tissue (Figure 4*C* and *D*), thus validating the results observed in the first cohort of patients. Cluster CD4-6 showed a profound nonfunctional phenotype because these cells did not produce any of the investigated cytokines, although other CD4$^+$ T cells did (Figure 4*E*). Remarkably, this T-cell subpopulation, compared with the ICOS$^-$ TIGIT$^-$ CD4$^+$ counterpart, showed high levels of the transcription factors Foxp3 ($P = .02$) and Helios ($P = .02$), but not of T-bet, and also expressed the proliferation marker Ki-67 ($P = .03$) within the tumor, suggesting an

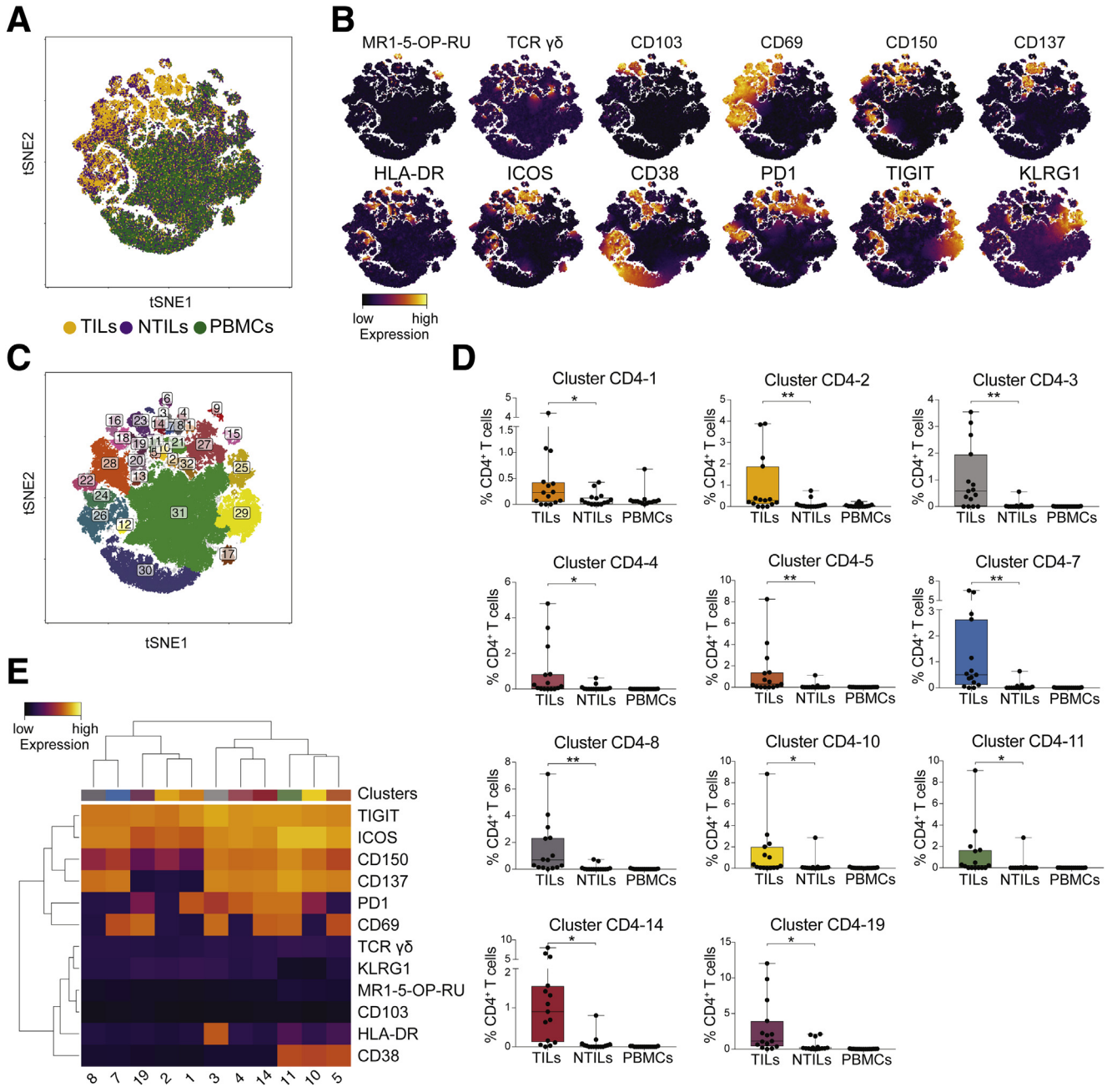

Figure 3. ICOS$^+$ TIGIT$^+$ CD4$^+$ T cells are enriched in TILs. (*A*) tSNE map of CD4$^+$ T cells in TILs (*yellow dots*), NTILs (*purple dots*), and PBMCs (*green dots*) of the first HCC cohort (n = 15). (*B*) tSNE maps showing the expression level and the distribution of each indicated marker. The color scale indicates the relative expression levels. (*C*) tSNE map of CD4$^+$ T cells with each cluster colored differently. (*D*) *Box plots* showing the frequency of CD4$^+$ T cells in each significantly enriched cluster in TILs vs NTILs. (*E*) Heatmap showing the normalized expression of the markers for selected clusters. The color scale indicates the relative expression levels. *$P \leq .05$ and **$P \leq .001$, Wilcoxon signed-rank test, adjusted with the Benjamini and Hochberg method.

activated phenotype (Figure 4*F*), in concordance with their expression of CD137 (Figure 4*E*).

Increased Frequency of CD38$^+$ PD1$^+$ CD8$^+$ T Cells in HCC

We next compared CD8$^+$ T cells in the 3 tissues (Figure 5*A*). Activated CD8$^+$ T cells preferentially accumulated in the tumor (Figure 5*B*), whereas CD8$^+$ MAIT and TCR $\gamma\delta$ cells showed similar expression in the investigated tissues (Figure 5*B*). Most of CD8$^+$ TILs expressed CD38 and PD1. Although cluster CD8-18 was enriched significantly in HCC ($P = .05$), clusters CD8-1, -2, -7, and -9, also containing CD38$^+$ PD1$^+$ CD8$^+$ T cells, were not (Figure 5*C* and *D*). Clusters CD8-1, -2, -7, and -9 also

Table 3. Cell Surface and Intracellular Staining Panel 2

Marker	Dye	Host species	Reactivity	Clone	Description	Catalog no
CD3	Alexa Fluor 700	Mouse	Human	UCHT1	Co-receptor: CD3 T cells	300424
CD4	PE	Mouse	Human	RPA-T4	Co-receptor: CD4 T cells	561843
CD8	BUV 496	Mouse	Human	RPA-T8	Co-receptor: CD8 T cells	564804
CD19	PE/Cy5	Mouse	Human	J3-119	Co-receptor: B cells	A07771
CD14	PE/Cy5	Mouse	Human	RMO52	Co-receptor: monocytes	A07765
CD137	PE/Dazzle	Mouse	Human	4B4-1	Costimulatory receptor	309826
CD278 (ICOS)	Brilliant Violet 510	Mouse	Human	C398.4A	Costimulatory receptor	313525
CD38	Brilliant Violet 650	Mouse	Human	HB-7	cADP ribose hydrolase	356620
TIGIT (VSTM3)	PerCP-eFluor 710	Mouse	Human	MBSA43	Inhibitory receptor	46-9500-42
PD1	Brilliant Violet 785	Mouse	Human	EH12.2H7	Inhibitory receptor	329930
IL22	PE	Mouse	Human	2G12A41	Proinflammatory cytokine	366704
TNF-α	PE/Cy7	Mouse	Human	MAb11	Proinflammatory cytokine	502930
IFN-γ	APC/Cy7	Mouse	Human	4S.B3	Proinflammatory cytokine	502530
Granzyme B	FITC	Mouse	Human/mouse	GB11	Cytotoxic molecule	515403
Perforin	Brilliant Violet 421	Mouse	Human	B-D48	Cytotoxic molecule	353307

cADP, cyclic adenosine diphosphate; DAPI, 4′,6-diamidino-2-phenylindole; FITC, fluorescein isothiocyanate; PE, phycoerythrin.

expressed the tissue-residence markers CD69 and/or CD103,[18,19] suggesting prolonged retention in HCC.[20]

The enrichment of PD1$^+$ CD8$^+$ T cells in HCC and the correlation of high PD1 levels with CD38 expression indicate the presence of previously activated cells, some of which could be tumor-specific within this cluster,[21] as also recently reported for non–small-cell lung cancer.[22]

Next, we compared the functional activities of CD8$^+$ T cells in TILs, NTILs, and PBMCs (Figure 6*A* and *B*). Seventeen clusters were identified (Figure 6*C*), of which 3 (clusters CD8-2, CD8-5, and CD8-7) showed accumulation in the tumor and contained CD38$^+$ PD1$^+$ CD8$^+$ T cells (Figure 6*D*). These 3 clusters showed variable production of IFN-γ, TNF-α, and granzyme B (Figure 6*E*), suggesting a proinflammatory role. CD38$^+$ PD1$^+$ cells were significantly more proliferating (Ki-67$^+$) than CD38$^-$ PD1$^-$ cells ($P = .04$) (Figure 6*F*), and showed similar expression of FoxP3, Helios, and T-bet transcription factors (Figure 6*F*). Taken together, these findings confirmed the presence within HCC of proliferating and functional CD38$^+$ PD1$^+$ cells, which might contribute to local inflammation and antitumor response.

Two Unique Populations of DN T Cells Are Present Within HCC

CD4$^-$ CD8$^-$ DN T cells contain different populations of innate-like T cells, including TCR $\gamma\delta$ and MAIT cells, and are more abundant in the liver than in PBMCs.[12,23] Multidimensional analysis of 10 markers (Figure 7*A* and *B*) showed 2 DN clusters significantly enriched in HCC biopsy specimens (Figure 7*C* and *D*). Cluster DN-6 contained activated CD38$^+$ TCR $\gamma\delta$ cells co-expressing the tissue-resident markers CD69 and CD103[17] and cluster DN-7 composed by TCR $\alpha\beta$ non-MAIT cells expressing the activation markers CD69, CD137, CD150, and HLA-DR, and the inhibitory TIGIT molecule (Figure 7*E*). Because CD137 is a marker of recent T-cell activation,[13] these findings suggest that a population of DN TCR $\alpha\beta$ cells might be activated within HCC.

Comparison of TIL Phenotype Correlates With Tumor Immunohistologic Profile

An important classification of tumors relies on the presence of mononuclear cell infiltrate (immune-inflamed, immune-excluded, and immune-desert) within tumor tissue.[6] To investigate potential correlations between the presence of immune infiltrate and unique cell clusters, each biopsy also was classified by H&E staining according to the immune infiltrate after recently proposed guidelines[24] (Figure 8). Nonsupervised hierarchical clustering identified 3 groups of CD4$^+$ TILs, 4 groups of CD8$^+$ TILs, and 4 groups of DN TILs (Figure 9*A*, *C*, and *E*, respectively). Next, we assessed the abundance of each group in inflamed vs noninflamed tumors (Figure 9*B*, *D*, and *F*). Within CD4$^+$ TILs, group 1 cells were accumulated significantly in inflamed tumors and were highly activated (Figure 9*B*). All cells co-expressed ICOS and TIGIT and, with some variability, other activation markers and inhibitory receptors. Group 2 cells lacked the CD69 marker and were enriched significantly in noninflamed tumors. Finally, group 3 included liver-resident T cells equally represented in inflamed and noninflamed tumors (Figure 9*A* and *B*).

Within CD8$^+$ TILs, 4 groups were identified. Group 1 cells contained resident memory CD8$^+$ TILs, co-expressed CD38, PD1, and TIGIT, together with both tissue-residence markers CD69 and CD103. Group 1 CD8$^+$ TILs were

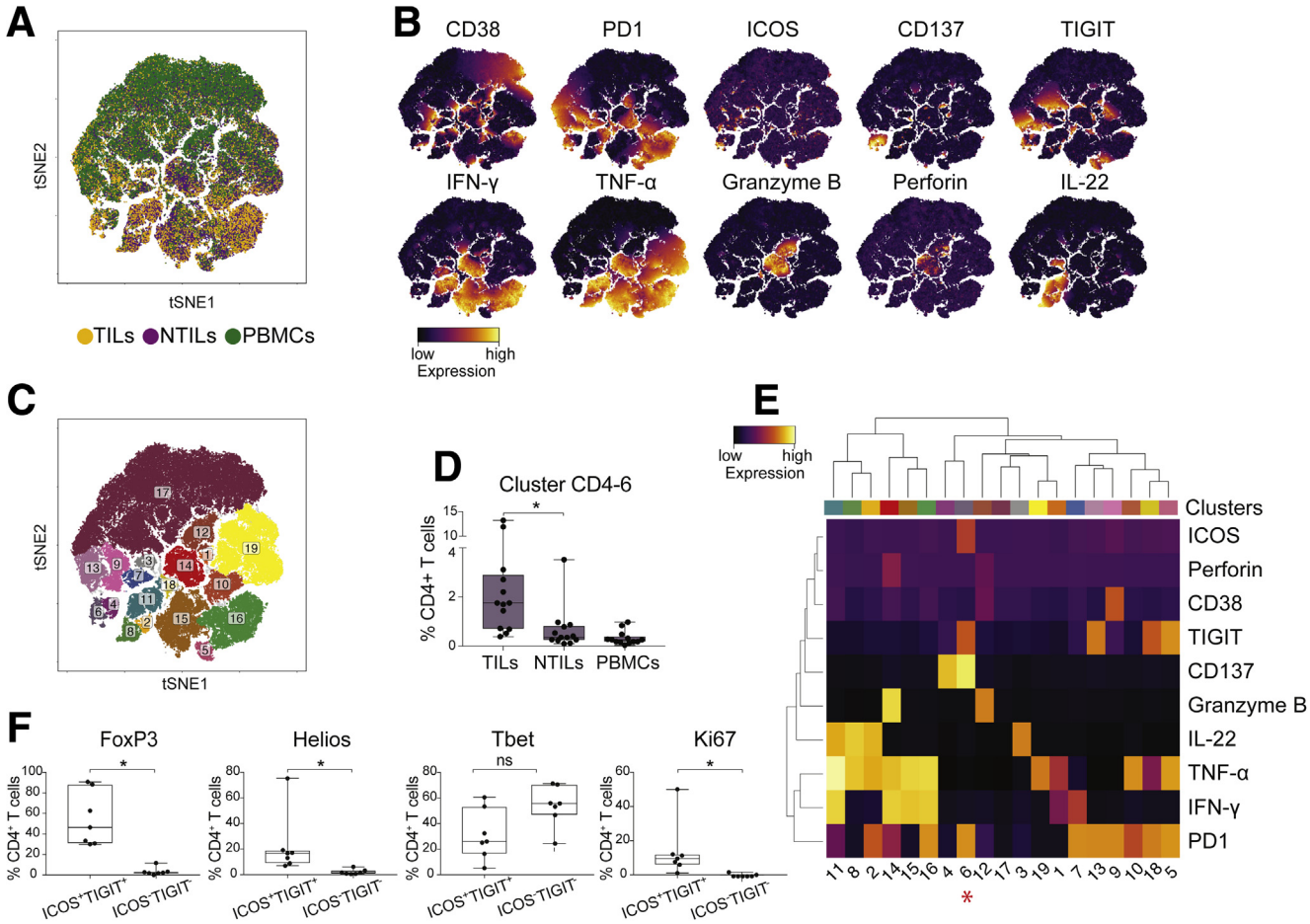

Figure 4. ICOS$^+$ TIGIT$^+$ CD4$^+$ T cells enriched in TILs are functionally impaired. (*A*) tSNE map of CD4$^+$ T cells in TILs (*yellow dots*), NTILs (*purple dots*), and TILs (*green dots*) of the second HCC cohort (n = 13). (*B*) tSNE maps showing the expression level and the distribution of each indicated marker. The color scale indicates the relative expression levels. (*C*) tSNE map with each cluster of CD4$^+$ T cells colored differently. (*D*) *Box plots* showing the frequency of CD4$^+$ T cells within cluster CD4-6 in TILs, NTILs, and PBMCs. (*E*) Heatmap showing the normalized expression of each marker in the indicated clusters. The color scale indicates the relative expression levels. * indicates cluster CD4-6, which is increased significantly in TILs vs NTILs. (*F*) *Box plots* showing the expression of indicated transcription factors on ICOS$^+$ TIGIT$^+$ CD4$^+$ and ICOS$^-$ TIGIT$^-$ CD4$^+$ TILs. *$P \leq .05$ and **$P \leq .01$, Wilcoxon signed-rank test, adjusted with the Benjamini and Hochberg method. ns, not significant.

enriched significantly in inflamed tumors, possibly as a result of local activation. Group 2 TILs identified liver-resident MAIT cells and group 4 identified liver-resident CD8$^+$ TILs. Both groups were not activated and were distributed equally among inflamed and noninflamed tumors. Finally, group 3 TILs contained CD8$^+$ T cells with a nonactivated and non–tissue-residence phenotype, and were enriched in noninflamed tumors (Figure 9*C* and *D*).

In DN TILs, group 1 contained MAIT cells, and group 2 contained both TCR $\alpha\beta$ and $\gamma\delta$ cells characterized by low expression of activation and tissue-residence markers. In contrast, group 3 contained activated CD150$^+$ DN cells and was enriched significantly in inflamed tumors. Finally, group 4 contained tissue-resident DN cells (Figure 9*E* and *F*). These findings showed that in HCC immune-inflamed tumors there are significantly increased populations of CD4$^+$, CD8$^+$, and DN TILs, which co-express unique markers of activation and tissue residence.

Phenotypic and Functional Changes of CD4$^+$ and CD8$^+$ T Cells in Tumor Biopsy Specimens Upon Nivolumab Treatment

Next, we examined the effects of the immune-checkpoint inhibitor nivolumab on TIL phenotype and function. Biopsy specimens before and during nivolumab therapy were studied in 7 HCC patients (Table 1, patients 4, 6, 19, 32, 34, 35, and 36, and Table 4 shows the list of analyzed molecules). We also found expression of CD38, ICOS, PD1 markers, and of IFN-γ, and IL13 cytokines and granzyme B in the TILs of these patients before treatment, as well as expression of the transcription factor T-bet (Figures 10*A* and *B* and 11*A* and *B*).

When we analyzed individual cell clusters (Figure 10*C*), an enrichment of activated and functionally impaired CD4$^+$ T cells was detected in TILs before treatment (cluster CD4-2; $P = .006$) (Figure 10*D* and *E*). Nivolumab therapy induced changes in the composition of

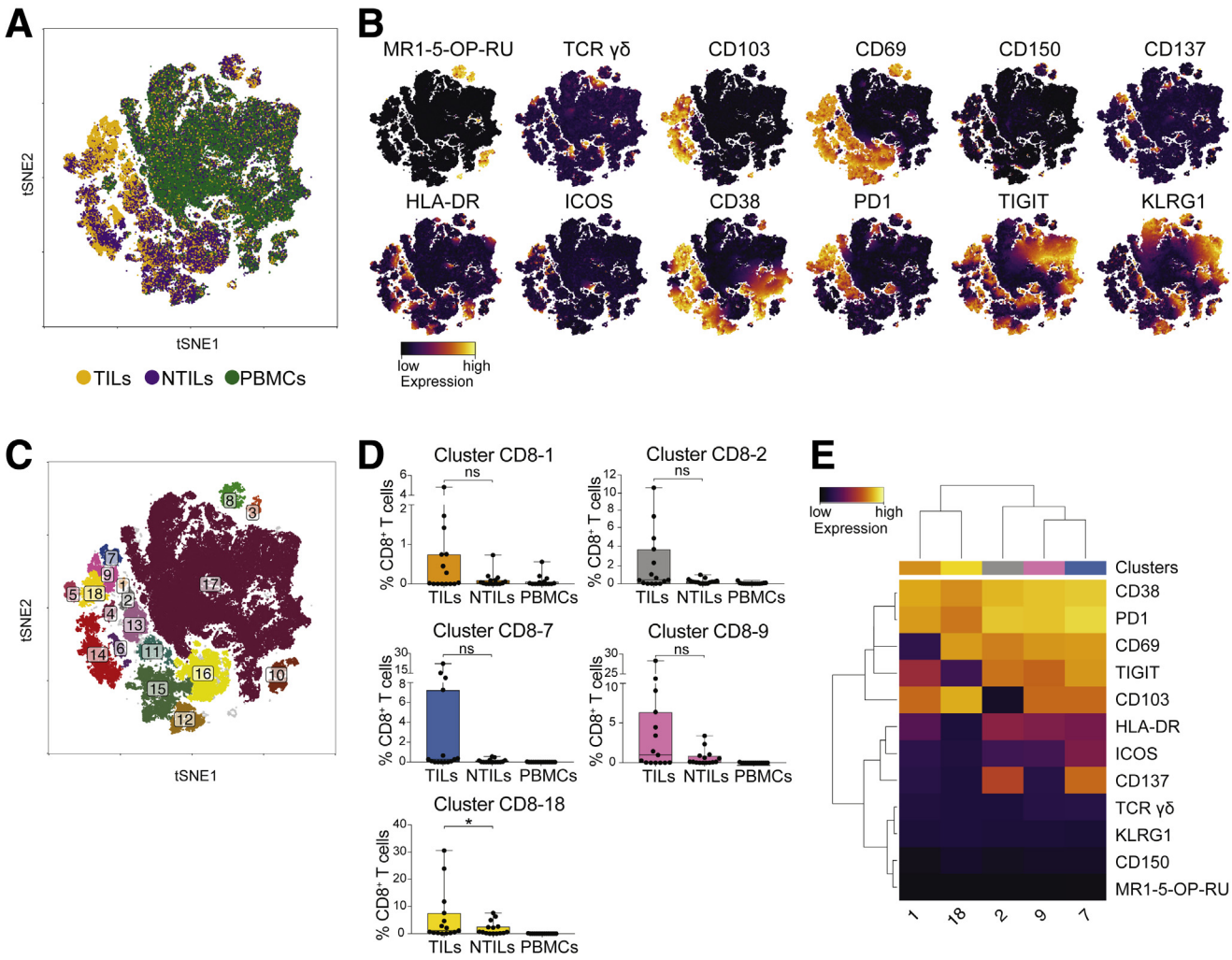

Figure 5. CD38$^+$ PD1$^+$ CD8$^+$ T cells are enriched in TILs. (*A*) tSNE map of CD8$^+$ T cells in TILs (*yellow dots*), NTILs (*purple dots*), and PBMCs (*green dots*). (*B*) tSNE maps showing the expression level and the distribution of each indicated marker. The color scale indicates the relative expression levels. (*C*) tSNE map with each cluster of CD8$^+$ T cells colored differently. (*D*) *Box plots* showing the frequency of CD8$^+$ T cells in each cluster significantly enriched in TILs. (*E*) Heatmap showing the normalized expression of the markers for the indicated clusters. The color scale indicates the relative expression levels. *$P \leq .05$, Wilcoxon signed-rank test, adjusted with the Benjamini and Hochberg method. ns, not significant.

CD4$^+$ and CD8$^+$ TIL clusters (Figure 12*A*, *B*, *E*–*G*), namely a reduced percentage of cells in cluster CD4-2 (ICOS$^+$ CD137$^+$ TIGIT$^+$ PD1$^+$ CD4$^+$ T cells), which, however, was not statistically significant ($P = .06$). Nivolumab therapy significantly reduced the percentage of cells in cluster CD4-10 ($P = .03$) that express RAR-related orphan receptor gamma T (RORγT) and T-bet and produce IFN-γ and IL13, while it increased the percentage of IFN-γ–producing CD38$^+$ CD4$^+$ T cells (cluster CD4-14; $P = .001$) (Figure 12*C* and *D*). Nivolumab therapy also promoted the enrichment of IFN-γ–producing CD38$^+$ CD8$^+$ T cells (cluster CD8-2; $P = .01$) (Figure 12*H* and *G*). Interestingly, in 2 patients with an immune-inflamed profile who responded to nivolumab, changes in patient-specific clusters of CD8$^+$ TILs were observed (Figure 13*A*–*H*). However, therapy-induced changes also were observed in a patient who did not respond to nivolumab (Figure 13*N*). Because not all patients with an immune-inflamed tumor profile responded to nivolumab, our data suggest that the presence of an immune-inflamed profile is necessary but not sufficient for clinical response to anti-PD1 immunotherapy. Because only 15% to 20% of HCC patients respond to nivolumab,[10] we could explain this low response rate by the high heterogeneity observed within tumor-infiltrating CD8$^+$ T cells.

Discussion

Tumor-infiltrating immune cells greatly contribute to therapy response and disease arrest.[25–29] Among the tumor infiltrating cell types, T lymphocytes directly participate in tumor killing and are considered favorable prognostic markers across multiple cancers.[7,8,30,31] However, the presence of a large number of TILs is not evidence of a

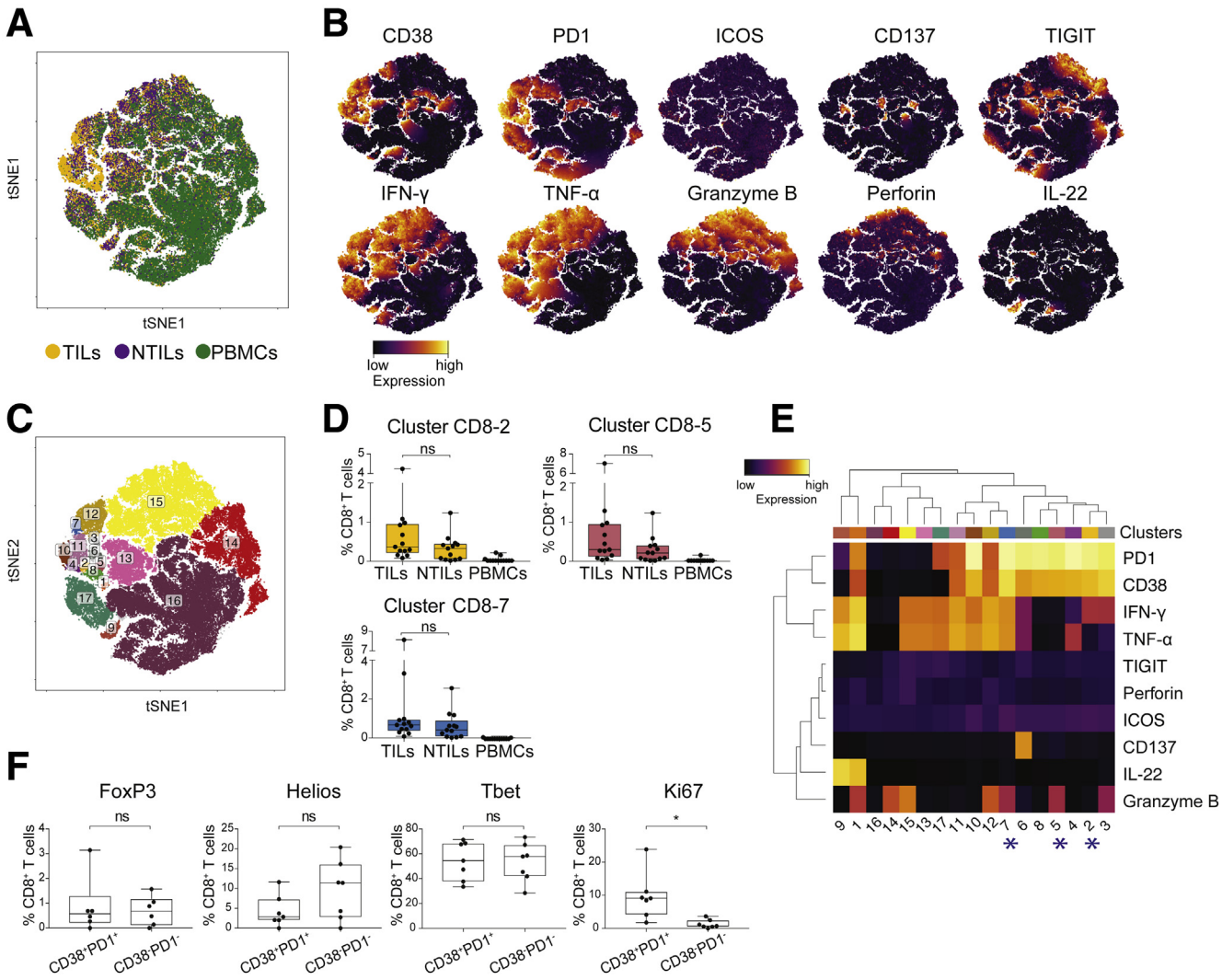

Figure 6. CD38$^+$ PD1$^+$ CD8$^+$ T cells enriched in TILs show different functionality. (*A*) tSNE map of CD8$^+$ T cells in TILs (*yellow dots*), NTILs (*purple dots*), and PBMCs (*green dots*). (*B*) tSNE maps show the expression level and the distribution of each indicated marker. Color scale indicates the relative expression levels. (*C*) tSNE map with each cluster of CD8$^+$ T cells colored differently. (*D*) *Box plots* show the frequency of the CD38$^+$ PD1$^+$ CD8$^+$ T-cell clusters increased in TILs. (*E*) Heatmap shows the normalized expression of each marker in the indicated clusters. Color scale indicates the relative expression levels. The * denote the clusters increased in TILs vs NTILs. (*F*) *Box plots* show the expression of the indicated transcription factor and proliferation marker in CD38$^+$ PD1$^+$ CD8$^+$ and CD38$^-$ PD1$^-$ CD8$^+$ TILs. Wilcoxon signed-rank test, adjusted with the Benjamini and Hochberg method. ns, not significant.

favorable prognosis because the status of T-cell activation, the expression of costimulatory and co-inhibitory molecules, and the functional capacity of TILs also contribute to the prognostic outcome.[32] Therefore, both TIL phenotype and functional properties are important to establish effective antitumor immunity.

In recent studies the TIL landscape in HCC has been investigated using different approaches.[33–36] Single-cell transcriptome studies were performed on small numbers of cells (<150 each in 6 HCC patients) and showed the presence of different CD8$^+$ populations expanded from a few precursors and characterized by exhausted and regulatory T cell (Treg) signatures.[33] A second study also showed the presence of a large numbers of both effector Tregs and CTLA-4$^+$ CD8$^+$ T cells in nonalcoholic steatohepatitis–related HCC patients, whereas large numbers of PD1$^+$CD8$^+$ T cells were observed in hepatitis B virus–related HCC patients.[34] In a third study, Treg and CD8$^+$ resident memory T cells were found enriched in a hepatitis B virus–related HCC microenvironment, which also was shown to contain more exhausted T cells than the microenvironment of non–viral-related HCC.[36] Despite these informative studies, a comprehensive assessment of phenotypic and functional T-cell populations in HCC still is lacking. In particular, it would be very important to identify which cell population(s) mediate an effective antitumor immune response at least in a group of HCC patients, and also to show the mechanisms contributing to immune-desert or immune-inflamed HCC. These factors might be useful to predict the response to immunotherapy.[37]

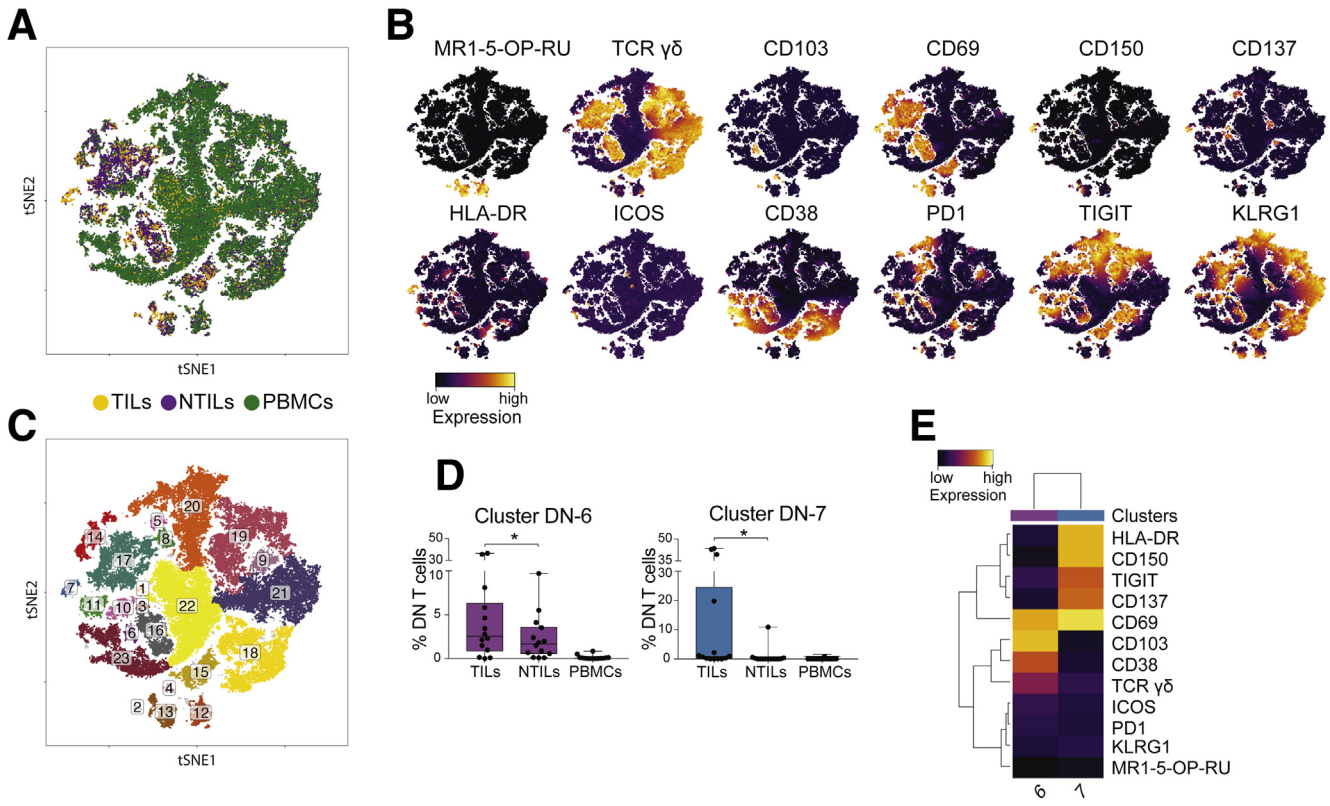

Figure 7. Unique clusters of DN T cells are enriched in TILs. (*A*) tSNE map of DN T cells in TILs (*yellow dots*), NTILs (*purple dots*), and PBMCs (*green dots*). (*B*) tSNE maps show the expression level and the distribution of each indicated marker. Color scale indicates the relative expression levels. (*C*) tSNE map with each cluster of DN T cells colored differently. (*D*) *Box plots* show the frequency of cells in each cluster significantly enriched in TILs. (*E*) Heatmap shows the normalized expression of the markers for the indicated clusters. Color scale indicates the relative expression levels. *$P \leq .05$, Wilcoxon signed-rank test, adjusted with the Benjamini and Hochberg method.

In the present study we performed multidimensional flow cytometric analysis of T cells isolated from tumor and nontumor liver biopsy specimens and from peripheral blood of HCC patients. These investigations provide several novel insights into the immune response to HCC.

First, the tumor environment was found to be enriched in $CD4^+$ T cells whereas $CD8^+$ T cells and DNs were more abundant in nontumor liver tissue, in agreement with data from transcriptomics studies.[33] We also found that TCR $\gamma\delta$ cells were less abundant in the tumor microenvironment than in normal liver, whereas MAIT cells were equally present. Whether these 2 populations of innate-like T cells have a role in the immune response to HCC remains open, although these findings seem to exclude local activation and recognition of tumor cells. On the contrary, a population of tumor-infiltrating $CD4^+$ T cells expressed CD137, a marker up-regulated in a transient manner upon T-cell antigen recognition.[38] $CD4^+$ cells also showed high expression of ICOS, an inducible costimulatory molecule expressed on previously activated T cells and T-follicular helper cells.[39] The presence of cells expressing both CD137 and ICOS markers might indicate that CD4-expressing cells are activated within the HCC microenvironment and perhaps recognize locally presented antigens. This possibility is in agreement with previous studies showing that $CD137^+$ cells isolated from ovarian cancers or melanomas are enriched in tumor-specific T cells.[31,40] The nature of the HLA class II–expressing antigen-presenting cells remains to be investigated, as does the identification of the antigens that stimulate $CD4^+$ cells within HCC.

Interestingly, we did not find an accumulation of $CD8^+$ or DN cells that expressed CD137, suggesting the absence of recent stimulation within HCC, or, alternatively, their unresponsive state.

A second finding was the presence of exclusive T-cell populations within HCC. The tSNE analyses showed the presence of unique $CD4^+$, $CD8^+$, and DN TILs, which were under-represented in NTILs and PBMCs. Within $CD4^+$ cells, ICOS and TIGIT-co-expressing cells were tumor-enriched. TIGIT is a co-inhibitory molecule present in activated T cells, and contributes to down-modulation of T-cell responses.[41] The co-expression of ICOS and TIGIT strongly suggest that $CD4^+$ cells activated within the tumor are probably becoming poor antigen-responders.[27] Most $ICOS^+$ and $TIGIT^+$ $CD4^+$ cells also expressed the CD137 marker, possibly suggesting recent antigen recognition. Finally, the majority of these cells also expressed the PD1 inhibitory

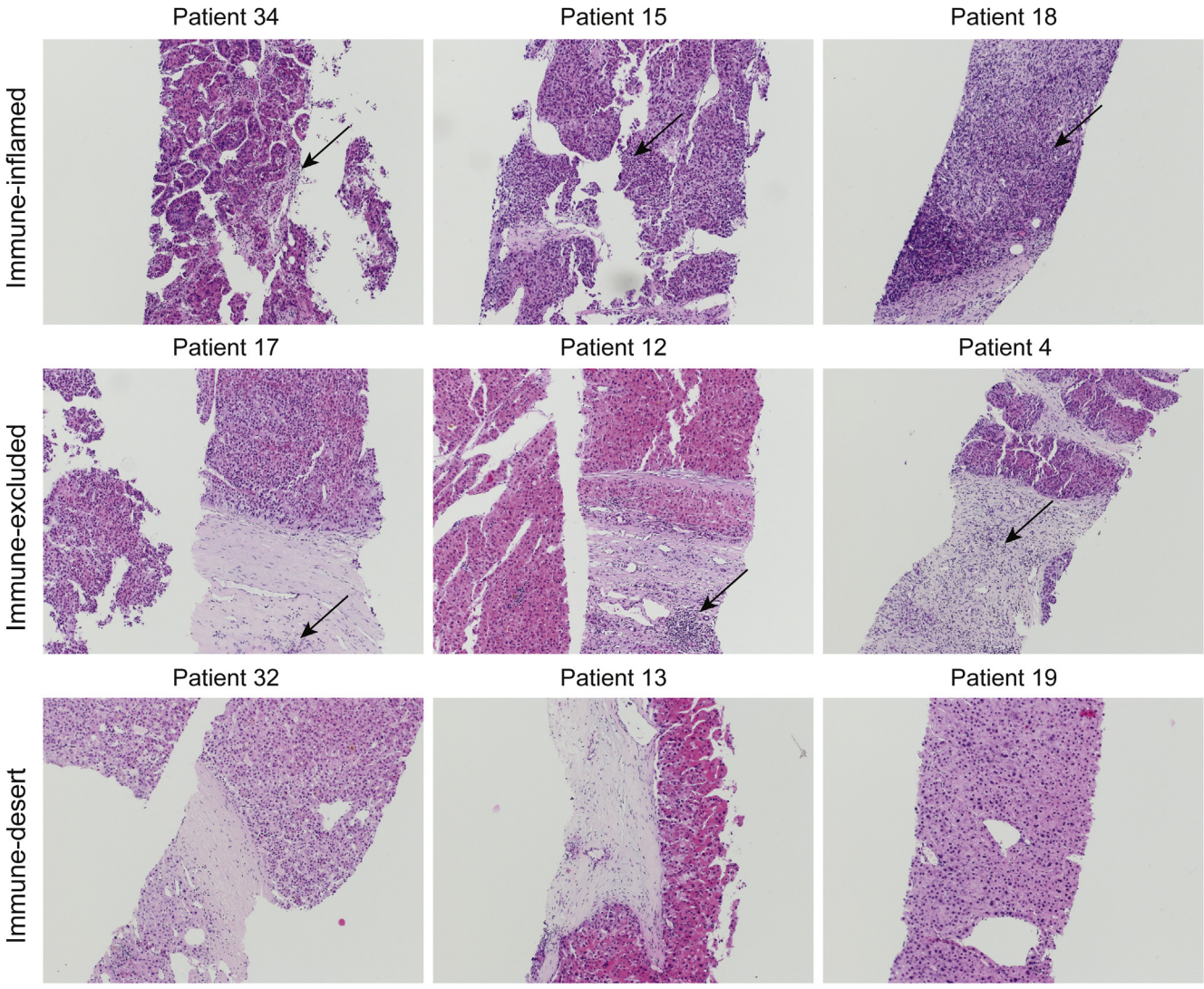

Figure 8. Representative histology of HCC tumors from 9 patients. (*A*) Immune-inflamed HCC with immune cells closely intermingled with tumor cells. (*B*) Immune-excluded HCC, showing ≥10% of the tumor stroma populated by immune cells located in the immediate vicinity of tumor cells. (*C*) Immune-desert HCC, showing less than 10% of the tumor stroma populated by lymphocytes, without dense immune cell infiltrates, and no contact of immune cells with tumor cells (original magnification, ×100, H&E stain). *Arrows* indicate the presence of lymphocytic infiltrates.

molecule. Although transient expression of inhibitory receptors is a characteristic of normal T-cell activation, the sustained expression of multiple immune checkpoint molecules is a hallmark of T-cell exhaustion after chronic stimulation by an antigen.[27] The latter possibility may be the case of this unique CD4 population, which showed a remarkable hyporesponsiveness and did not produce cytokines upon stimulation, even with PMA + ionomycin. Not all cells co-expressing PD1 and TIGIT were functionally impaired, suggesting that only some cells were chronically stimulated within the tumor.[42]

Recent studies described the increased frequency of $ICOS^+$ $FoxP3^+$ Tregs in HCC[43] and, more recently, a single-cell transcriptomics study proposed a unique HCC-infiltrating Tregs gene signature[33] that overlapped with signatures in melanoma, breast, colon, and lung cancers.[44–46] In accordance with these publications, our studies detected a high percentage of FoxP3- and Helios-expressing T cells within $ICOS^+$ $TIGIT^+$ $CD4^+$ TILs, which could indicate a regulatory function. However, FoxP3 and ICOS markers also are expressed by recently stimulated T cells, and thus these cells might represent T cells responding to antigen within the tumor. Because of the extremely small number of this population in the biopsy specimens and lack of information on antigen specificity, it was not possible to sort these cells and test their putative inhibitory function.

In HCC biopsy specimens we also found unique clusters of $CD38^+$, $PD1^+$, and $CD8^+$ TILs, which proliferated and expressed inflammatory (TNF-α and IFN-γ) cytokines and cytotoxic (granzyme B) molecules upon stimulation. These cells showed a high interpatient heterogeneity that

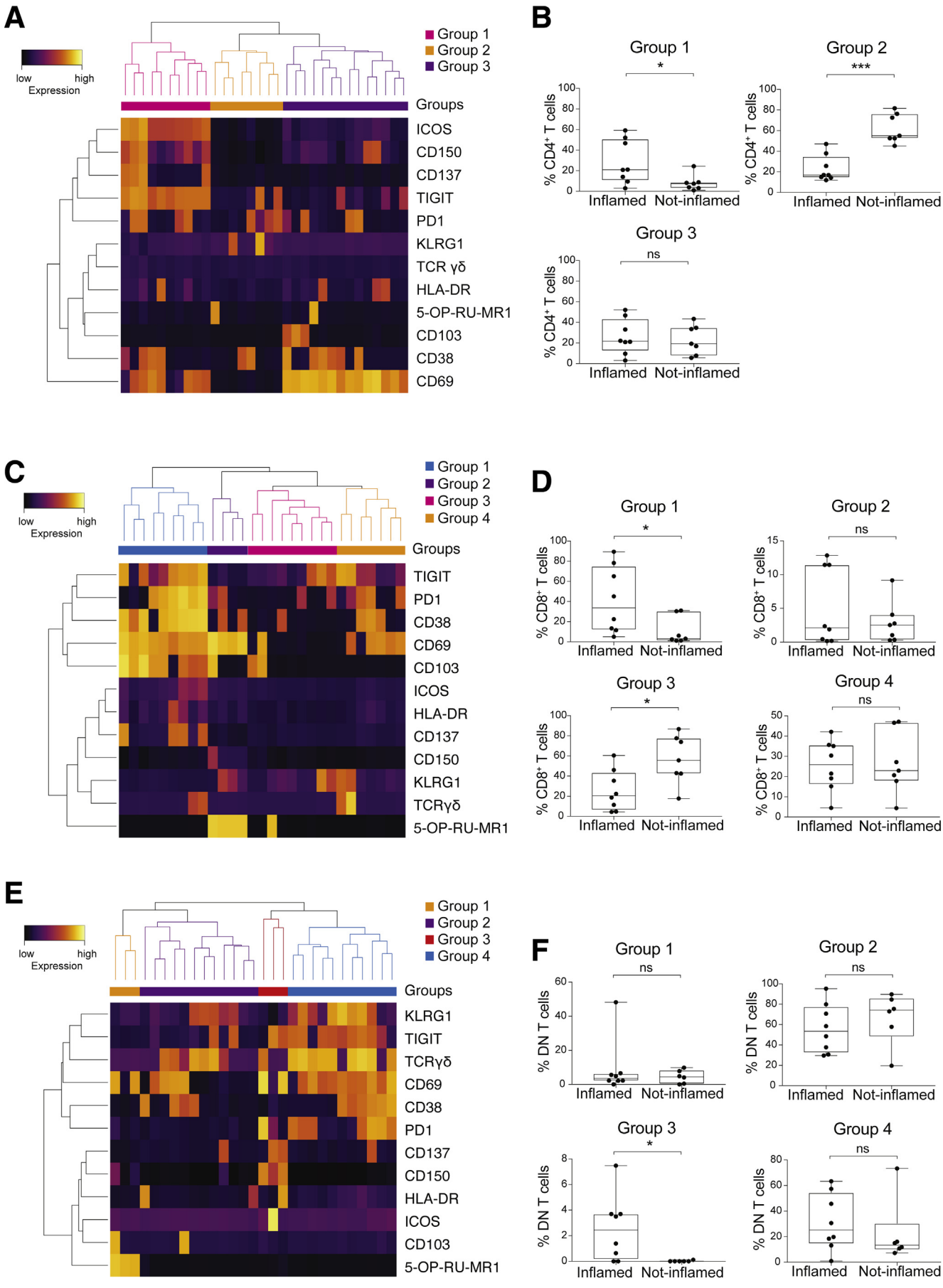
A
low
high
Expression
Group 1
Group 2
Group 3
Groups
ICOS
CD150
CD137
TIGIT
PD1
KLRG1
TCR γδ
HLA-DR
5-OP-RU-MR1
CD103
CD38
CD69
B
Group 1
*
Group 2
***
Group 3
ns
% CD4+ T cells
Inflamed
Not-inflamed
C
Group 1
Group 2
Group 3
Group 4
Groups
TIGIT
PD1
CD38
CD69
CD103
ICOS
HLA-DR
CD137
CD150
KLRG1
TCRγδ
5-OP-RU-MR1
D
% CD8+ T cells
E
KLRG1
TIGIT
TCRγδ
CD69
CD38
PD1
CD137
CD150
HLA-DR
ICOS
CD103
5-OP-RU-MR1
F
% DN T cells

Table 4. Cell Surface and Intracellular Staining Panel 4

Marker	Dye	Host species	Reactivity	Clone	Description	Catalog no
CD3	Alexa Fluor 700	Mouse	Human	UCHT1	Co-receptor: CD3 T cells	300424
CD4	Brilliant Violet 711	Mouse	Human	OKT4	Co-receptor: CD4 T cells	317440
CD8	BUV 496	Mouse	Human	RPA-T8	Co-receptor: CD8 T cells	564804
CD19	PE/Cy5	Mouse	Human	J3-119	Co-receptor: B cells	A07771
CD14	PE/Cy5	Mouse	Human	RMO52	Co-receptor: monocytes	A07765
CD137	PE/Dazzle 594	Mouse	Human	4B4-1	Costimulatory receptor	309826
CD278 (ICOS)	Brilliant Violet 510	Mouse	Human	C398.4A	Inhibitory receptor	313525
CD38	Brilliant Violet 650	Mouse	Human	HB-7	cADP ribose hydrolase	356620
PD1	Brilliant Violet 785	Mouse	Human	EH12.2H7	Inhibitory receptor	329930
IFN-γ	APC/Cy7	Mouse	Human	4S.B3	Proinflammatory cytokine	502530
IL13	PE/Cy7	Mouse	Human	JES10-5A2	Proinflammatory cytokine	501914
Granzyme B	FITC	Mouse	Human/mouse	GB11	Cytotoxic molecule	515403
T-bet	PE	Mouse	Human	4B10	Transcription factor–Th1 polarized T cell	137236
GATA-3	Brilliant Violet 711	Mouse	Human	16E10A23	Transcription factor–Th2 polarized T cell	653814
RORγt	APC	Mouse	Human/mouse	AFKJS-9	Transcription factor–Th17 polarized T cell	17-6988-80

cADP, cyclic adenosine diphosphate; FITC, fluorescein isothiocyanate; PE, phycoerythrin.

probably contributes to the high variability in tumor immunity.

The liver is an organ containing several innate immune cell populations.[47] Among these, there is enrichment of unconventional T cells, including MAIT, TCR $\gamma\delta$ T and DN TCR $\alpha\beta$ T cells[12,47,48] that recognize nonpeptide ligands presented by non–major histocompatibility complex antigen-presenting molecules.[49] Their antitumor activity recently has been debated.[50,51]

In HCC, we found an enrichment of activated TCR $\gamma\delta$ cells expressing CD38, CD69, and CD103 markers. The antigens and the presenting molecules stimulating $\gamma\delta$ cells in HCC remain unknown and might provide useful information to further investigate recruitment and antitumor activity of TCR $\gamma\delta$ cells in HCC.

A second significantly increased TIL population was CD4-CD8 DN and expressed a TCR $\alpha\beta$ together with the activation markers CD137, HLA-DR, and CD69. These cells also up-regulated $CD150^+$, a costimulatory molecule present in activated lymphocytes and facilitating efficient T- and B-cell responses.[52] The expression of all such activation markers is a strong indication that unconventional T cells also might become stimulated within HCC. The identification of the stimulatory antigens may provide unexpected information to anti-HCC immunity and may designate these DN T cells as a novel immunotherapy target population.

Our study also provided 2 additional facts. The first is the correlation of the presence of exclusive T cells with currently adopted histologic classification. Immune inflamed tumors showed an increase of unique HCC-specific $CD4^+$, $CD8^+$, and DN TILs. Importantly, these cells expressed markers of activation and tissue residence, possibly suggesting activation within the tumor.

On the contrary, in immune-excluded tumors there was a large number of cells lacking activation and tissue-residence markers, probably reflecting recent blood extravasation. These findings support the clinical relevance of the histologic classification and identify novel markers to recognize nonfunctional TILs in HCC.

The second additional fact is regarding the effects of nivolumab therapy on HCC TILs. Phases 1–2 clinical studies have shown that nivolumab treatment induces a tumor reduction and an objective patient response to the therapy in 15%–20% of patients with advanced HCC.[10] Based on our findings on nontreated HCC patients, we aimed to characterize the effects of anti-PD1 immunotherapy on the phenotype and function of the unique populations of HCC TILs. Although significant variations in the frequency of total T cells were not observed,

Figure 9. (***See previous page***). **TIL clusters correlate with tumor microenvironment.** (*A*) Heatmap showing the normalized expression of the indicated markers for each $CD4^+$ TIL cluster. The color scale indicates the relative expression levels. (*B*) *Box plots* showing the frequency of $CD4^+$ TIL groups in inflamed tumors (immune-inflamed tumors) vs noninflamed tumors (immune-excluded and immune-desert tumors). (*C*) Heatmap showing the normalized expression of the markers for each $CD8^+$ TIL cluster. The color scale indicates the relative expression levels. (*D*) *Box plots* showing the frequency of $CD8^+$ TIL groups in inflamed tumors (immune-inflamed tumors) vs noninflamed tumors (immune-excluded and immune-desert tumors). (*E*) Heatmap showing the normalized expression of the markers for each DN TIL cluster. The color scale indicates the relative expression levels. (*F*) *Box plots* showing the frequency of DN TIL groups in inflamed tumors (immune-inflamed tumors) vs noninflamed tumors (immune-excluded and immune-desert tumors).

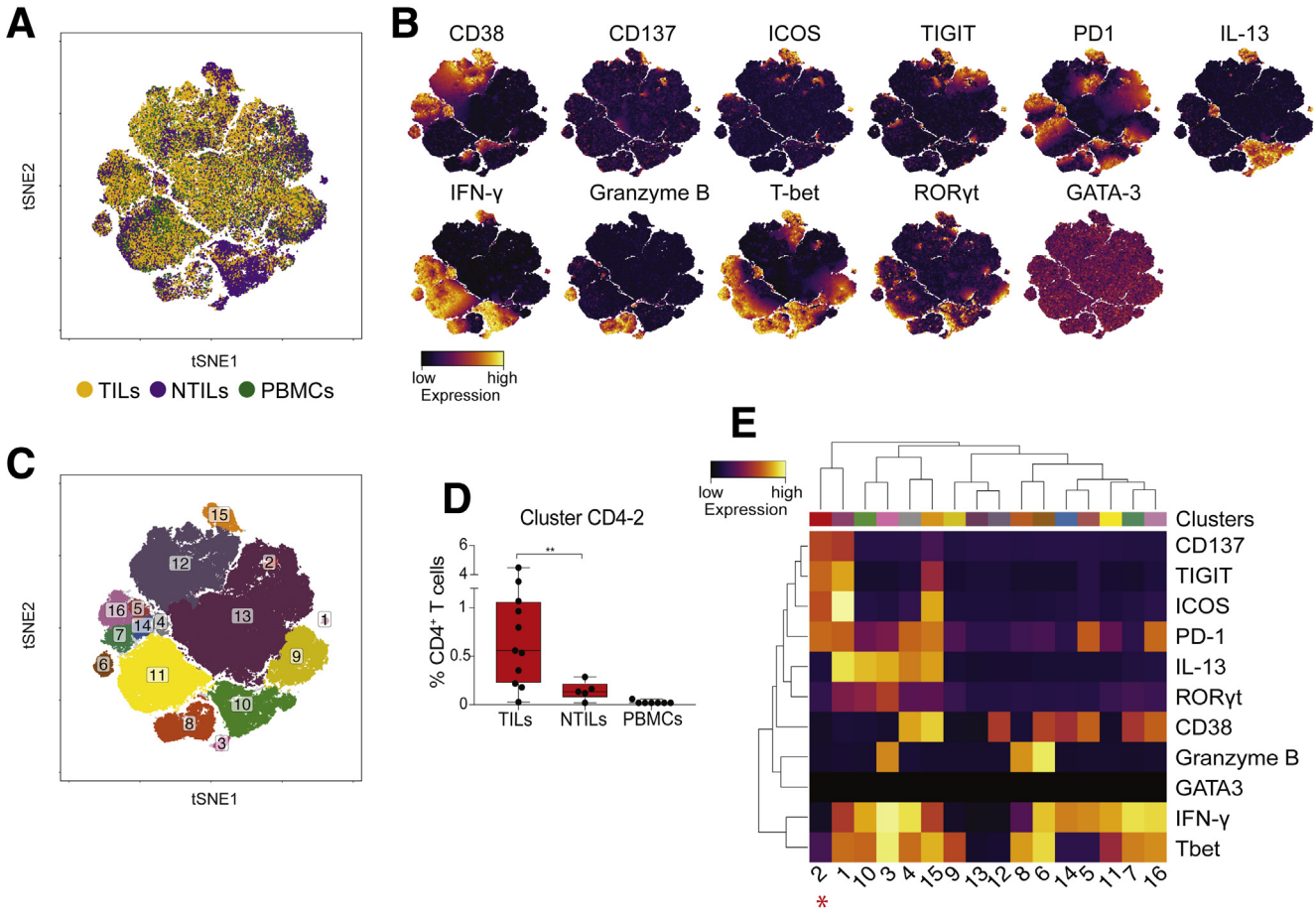

Figure 10. ICOS$^+$ TIGIT$^+$ PD1$^+$ CD137$^+$ CD4$^+$ T cells are enriched in patients before treatment. (*A*) tSNE map of CD4$^+$ T cells from TILs (*yellow dots*), NTILs (*purple dots*), and PBMCs (*green dots*) of pretreatment and on-therapy HCC patients. (*B*) tSNE maps show the expression level and the distribution of each indicated marker. Color scale indicates the relative expression levels. (*C*) tSNE map colored by clusters of CD4$^+$ T cells. (*D*) *Box plot* shows the frequency of the ICOS$^+$ TIGIT$^+$ PD1$^+$ CD137$^+$ CD4$^+$ T-cell cluster significantly enriched in pretreatment HCC biopsy specimens. (*E*) Heatmap shows the normalized expression of the panel markers for the indicated clusters. Color scale indicates the relative expression levels. The *red asterisk* denotes the cluster 2 significantly increased in TILs vs NTILs.

important changes of HCC unique TILs were detected. The effects on circulating lymphocytes and NTILs were minimal, whereas drastic changes were observed in TILs because they diminished unresponsive ICOS$^+$ TIGIT$^+$ CD4$^+$ T cells and increased activated CD4$^+$ and CD8$^+$ T cells expressing CD38 and producing IFN-γ. Thus, in HCC, anti-PD1 treatment promotes the reduction of unresponsive T cells and establishment of an inflamed tumor microenvironment. The increased IFN-γ release might modulate both immune and tumor cell functions,[53,54] thus positively influencing antitumor immunity. These preliminary findings could indicate that the histologic enumeration of ICOS$^+$ TIGIT$^+$ CD4$^+$ TILs in inflamed HCC represents a prognostic indicator of therapy responsiveness. However, this possibility has to be considered with caution. Indeed, we are aware that the analysis described here is based on a small number of patients and that validation of its prognostic value requires ad hoc prospective studies that include more patients.

In conclusion, our detailed characterization of HCC-infiltrating TILs showed a unique populations of locally activated T cells that may provide effective antitumor immunity. These studies set the point for the identification of the tumor antigens stimulating these T cells and their possible exploitation as immunotherapeutic targets in HCC.

Materials and Methods

Patient Samples

Blood and liver needle biopsy specimens from HCC patients (n = 36) (Table 1) were obtained in the outpatient clinic of the Division of Gastroenterology and Hepatology at the University Hospital Basel (Basel, Switzerland). The use of biopsy material for this project was approved by the ethics committee of the northwestern part of Switzerland (protocol EKNZ 2014-099).

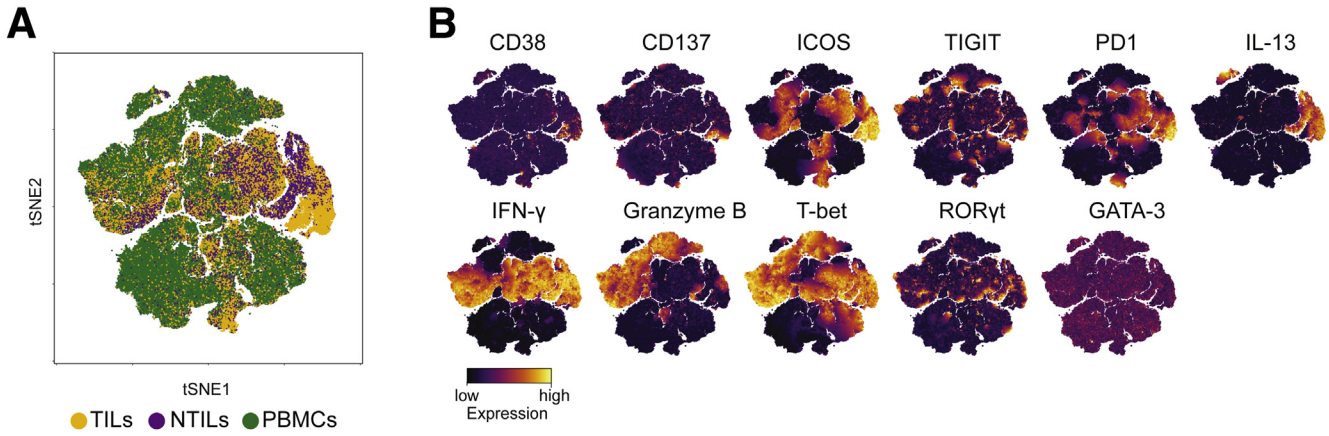

Figure 11. Nivolumab therapy affects CD8$^+$ T-cell phenotype. (*A*) tSNE map of CD8$^+$ T cells from TILs (*yellow dots*), NTILs (*purple dots*), and PBMCs (*green dots*) of pretreated and on-therapy HCC patients. (*B*) tSNE maps showing the expression level and the distribution of each indicated marker. Color scale indicates the relative expression levels.

Histology

Liver biopsy specimens were fixed in 10% buffered formalin and embedded in paraffin. Sections were stained with H&E. Histopathologic evaluation was assessed by a board-certified pathologist (L.T.). Tumors were classified histologically according to the Edmondson–Steiner grading system and according to their immune-phenotype.[55] In our HCC cohort, 3 patterns were described as follows: (1) immune-desert tumors, in which less than 10% of tumor stroma was populated by lymphocytes, and no dense immune cell infiltrates or contacts of the immune cells with tumor cells were detected; (2) immune-excluded tumors, in which ≥10% of tumor stroma was populated by lymphocytes located in the immediate vicinity of tumor cells; and (3) immune-inflamed, if lymphocytes were present in the tumor parenchyma in close proximity to tumor cells. This classification was not immediately applicable in every case because some tumors showed certain degrees of overlap between the different patterns described. In such cases, the tumors were classified according to the most prevalent pattern. Necrotic areas were excluded from evaluation. Macrophages and granulocytes were not considered for this classification. Our HCC cohort included prevalently biopsy specimens with an immune-inflamed phenotype.

PBMCs and Liver Infiltrating Immune Cells

PBMCs were isolated from 15 mL of blood by standard density-gradient centrifugation protocols, washed twice in phosphate-buffered saline (PBS), and cryopreserved in medium containing 90% fetal bovine serum and 10% dimethyl sulfoxide until fluorescence-activated cell sorter analysis. For isolation of liver-infiltrating lymphocytes, cylinders of liver biopsy specimens (diameter, ~1 mm; length, 2 cm) were obtained from tumor and nontumor liver of HCC patients. The samples were washed in PBS to avoid blood contamination and mechanically smashed above a cell strainer (40-mm nylon). The recovered cells were washed twice in PBS and cryopreserved.

Antibodies

The primary monoclonal antibodies and MHC class I-related molecule (MR1) tetramers used are described in Table 5.

Intracellular Cytokine Induction

Liver infiltrating lymphocytes and PBMCs were thawed in PBS with 10 μg/mL DNase I (Sigma-Aldrich, St. Louis, MO) to prevent cell clumping. The cells were resuspended in RPMI 1640 medium (Gibco, Gaithersburg, MD) supplemented with 10% heat-inactivated fetal bovine serum (Bioconcept, 4123 Allschwil, CH), 100 U/mL kanamycin, 2 mmol/L stable glutamine, 1 mmol/L sodium pyruvate, and 1% minimal essential medium (MEM) nonessential amino acids (all from Bioconcept), and 10 μg/mL DNase I. The cells were rested for 1 hour at 37°C before further processing. For intracellular cytokine induction, the cells were washed and resuspended in complete medium containing PMA (25 ng/mL), calcium ionophore ionomycin (1 μg/mL), and Brefeldin A (10 μg/mL; all from Sigma-Aldrich) for 4 hours. The LIVE/DEAD Fixable Aqua Dead Cell Stain Kit (Invitrogen, Norcross, GA) was used to identify viable cells before intracellular staining.

Flow Cytometry

Liver-infiltrating lymphocytes and PBMCs were washed and resuspended in blocking buffer (PBS containing 50% human serum) for 30 minutes at room temperature.

Cells were resuspended in staining buffer (PBS containing 0.02% NaN_3 and 0.5% human albumin) and stained with MR1 tetramers (National Institutes of Health Tetramer Core Facility, Emory University, Atlanta, GA) for 40 minutes at room temperature, followed by other surface stains for 20 minutes at 4°C in the dark. For intracellular staining, cells

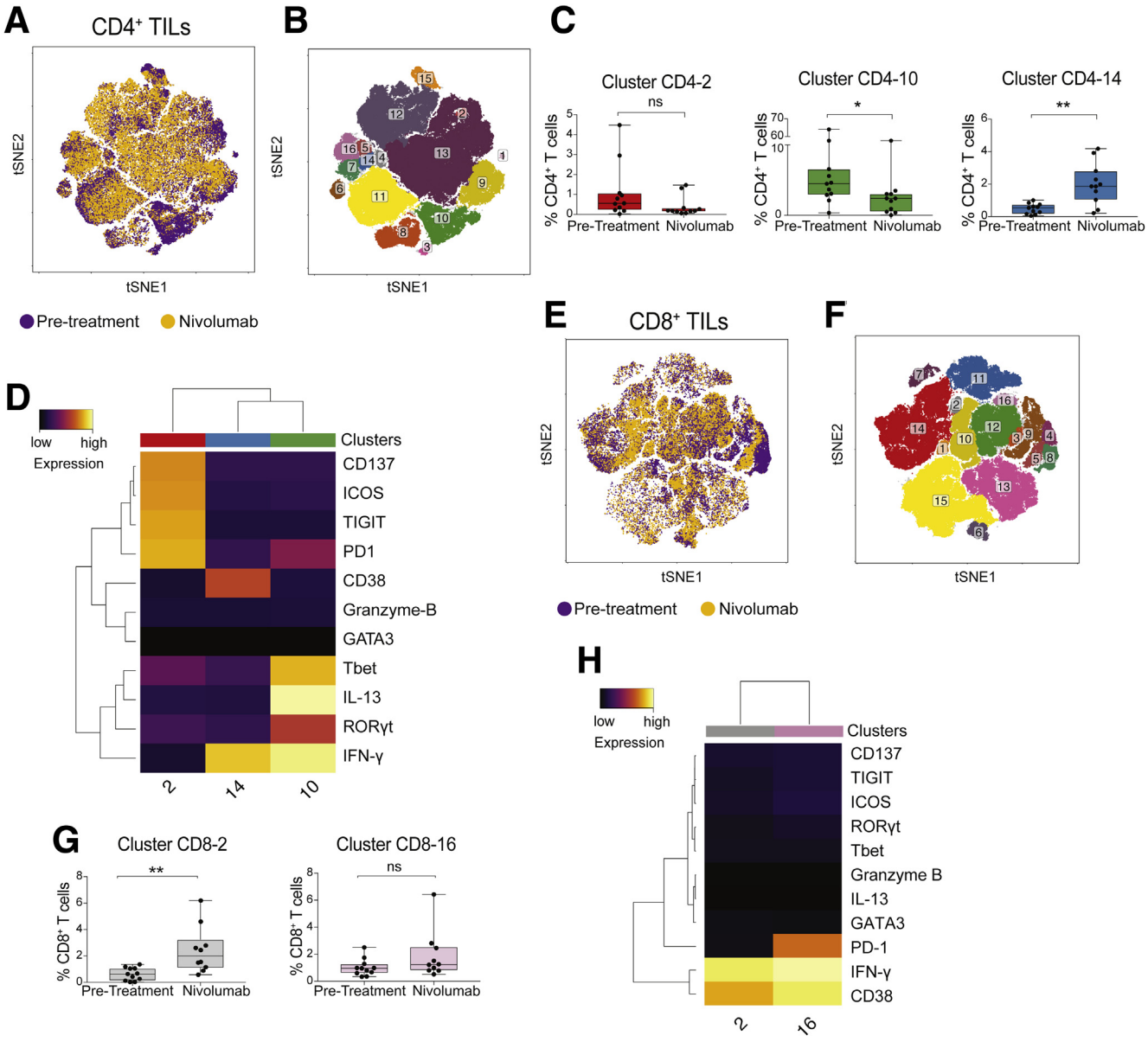

Figure 12. Nivolumab therapy reduces the frequency of exhausted CD4$^+$ T cells in TILs and increases the frequency of activated CD4$^+$ and CD8$^+$ TILs producing IFN-γ. (*A*) tSNE map of CD4$^+$ T cells infiltrating the tumor in samples before treatment (*purple dots*) and on-treatment with nivolumab (*yellow dots*). (*B*) tSNE map colored by clusters in CD4$^+$ TILs. (*C*) *Box plots* showing the frequency CD4$^+$ TIL clusters before and on nivolumab therapy. (*D*) Heatmap of the CD4$^+$ TIL clusters changed after nivolumab therapy. The heatmap shows the normalized expression of the panel markers. The color scale indicates the relative expression levels. (*E*) tSNE map of CD8$^+$ T cells infiltrating the tumor samples before treatment (*purple dots*) and on-treatment with nivolumab (*yellow dots*). (*F*) tSNE map colored by clusters of CD8$^+$ TILs. (*G*) *Box plots* showing the frequency of CD8$^+$ TIL clusters before and on nivolumab therapy. (*H*) Heatmap of the CD8$^+$ TIL clusters changed after nivolumab therapy. The heatmap shows the normalized expression of the panel markers. The color scale indicates the relative expression levels. *$P \leq .05$ and **$P \leq .001$, Wilcoxon signed-rank test, adjusted with the Benjamini and Hochberg method. ns, not significant.

subsequently were washed in staining buffer twice before fixation and permeabilization using Biolegend (San Diego, CA) buffers for intracellular staining. In short, cells were suspended in the fixation buffer in the dark for 30 minutes, washed with permeabilization wash buffer, and stained for intracellular markers for 20 minutes at 4°C in the dark. Samples were analyzed on LSR Fortessa flow (BD Bioscience, San Jose, CA).

Flow Cytometry Data Analysis

Flow cytometry data were analyzed using FlowJo v10.1 software (TreeStar, 2060 Antwerpen, Belgium), before exporting to R, and transformed using an inverse hyperbolic sine function. Dimensionality reduction was performed on transformed data with the Barnes–Hutt implementation of tSNE,[56] using a custom R script (available on request). For each set of analyses, individual

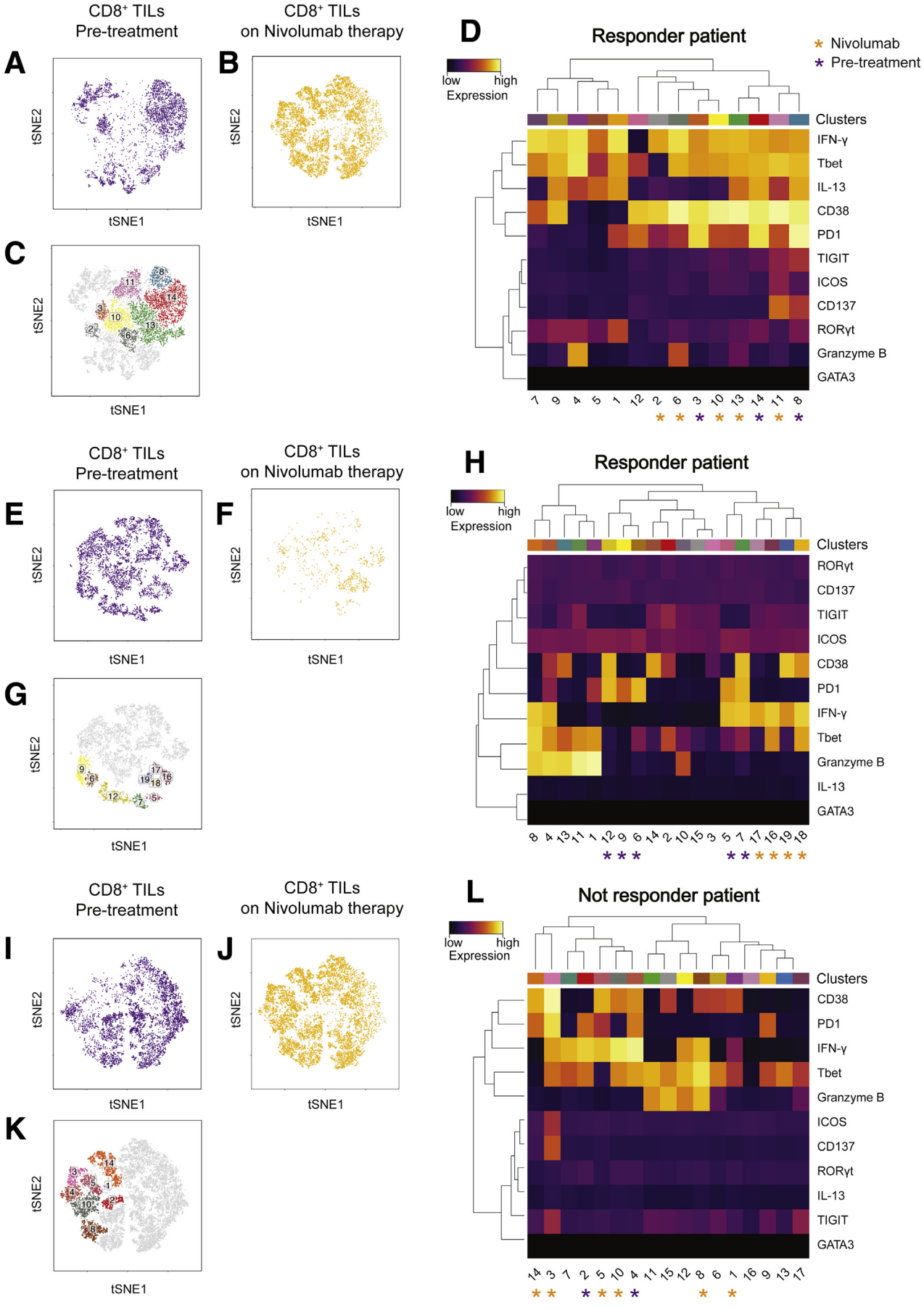
A
CD8+ TILs
Pre-treatment
tSNE2
tSNE1
B
CD8+ TILs
on Nivolumab therapy
tSNE2
tSNE1
C
tSNE2
tSNE1
D
Responder patient
low
high
Expression
Nivolumab
Pre-treatment
Clusters
IFN-γ
Tbet
IL-13
CD38
PD1
TIGIT
ICOS
CD137
RORγt
Granzyme B
GATA3
7 9 4 5 1 12 2 6 3 10 13 14 11 8
E
CD8+ TILs
Pre-treatment
tSNE2
tSNE1
F
CD8+ TILs
on Nivolumab therapy
tSNE2
tSNE1
G
tSNE2
tSNE1
H
Responder patient
low
high
Expression
Clusters
RORγt
CD137
TIGIT
ICOS
CD38
PD1
IFN-γ
Tbet
Granzyme B
IL-13
GATA3
8 4 13 11 1 12 9 6 14 2 10 15 3 5 7 17 16 19 18
I
CD8+ TILs
Pre-treatment
tSNE2
tSNE1
J
CD8+ TILs
on Nivolumab therapy
tSNE2
tSNE1
K
tSNE2
tSNE1
L
Not responder patient
low
high
Expression
Clusters
CD38
PD1
IFN-γ
Tbet
Granzyme B
ICOS
CD137
RORγt
IL-13
TIGIT
GATA3
14 3 7 2 5 10 4 11 15 12 8 6 1 16 9 13 17

Table 5. Reagents

Marker	Dye	Host species	Reactivity	Clone	Company	Catalog no
CD3	PE/Cy7	Mouse	Human	UCHT1	Biolegend	300420
CD3	Alexa Fluor 700	Mouse	Human	UCHT1	Biolegend	300424
TCR $\gamma\delta$	Brilliant Violet 421	Mouse	Human	B1	Biolegend	331218
CD4	Brilliant Violet 711	Mouse	Human	OKT4	Biolegend	317440
HLA-DR	Alexa Fluor 700	Mouse	Human	L243	Biolegend	307626
CD38	Brilliant Violet 650	Mouse	Human	HB-7	Biolegend	356620
CD137	PE/Dazzle 594	Mouse	Human	4B4-1	Biolegend	309826
CD278 (ICOS)	Brilliant Violet 510	Mouse	Human	C398.4A	Biolegend	313525
CD150 (SLAM)	FITC	Mouse	Human	A12 (7D4)	Biolegend	306306
CD69	APC/Cy7	Mouse	Human	FN50	Biolegend	310914
CD103	APC	Mouse	Human	Ber-ACT8	Biolegend	350216
PD1	Brilliant Violet 785	Mouse	Human	EH12.2H7	Biolegend	329930
KLRG1	Brilliant Violet 605	Mouse	Human	2F1/KLRG1	Biolegend	138419
TIGIT (VSTM3)	Brilliant Violet 605	Mouse	Human	A15153G	Biolegend	372706
IL22	PE	Mouse	Human	2G12A41	Biolegend	366704
TNF-α	PE/Cy7	Mouse	Human	MAb11	Biolegend	502930
IFN-γ	APC/Cy7	Mouse	Human	4S.B3	Biolegend	502530
T-bet	PE	Mouse	Human	4B10	Biolegend	137236
Granzyme B	FITC	Mouse	Human/mouse	GB11	Biolegend	515403
Perforin	Brilliant Violet 421	Mouse	Human	B-D48	Biolegend	353307
Helios	PE/Cy7	Mouse	Human	22F6	Biolegend	137236
Foxp3	Alexa Fluor 647	Mouse	Human	150D	Biolegend	320014
IL13	PE/Cy7	Mouse	Human	JES10-5A2	Biolegend	501914
GATA-3	Brilliant Violet 711	Mouse	Human	16E10A23	Biolegend	653814
Ki-67	Alexa 488	Mouse	Human	Ki-67	Biolegend	350508
CD19	PE/Cy5	Mouse	Human	J3-119	Beckman Coulter (1260 Nyon, France)	A07771
CD14	PE/Cy5	Mouse	Human	RMO52	Beckman Coulter	A07765
CD4	PE	Mouse	Human	RPA-T4	BD Bioscience (60322 Frankfurt am Main, Germany)	561843
CD4	APC	Mouse	Human	RPA-T4	BD Bioscience	555349
CD8	BUV 496	Mouse	Human	RPA-T8	BD Bioscience	564804
TIGIT (VSTM3)	PerCP-eFluor 710	Mouse	Human	MBSA43	eBioscience	46-9500-42
ROR-γt	APC	Mouse	Human/mouse	AFKJS-9	eBioscience	17-6988-80
hMR1-5OP-RU tetramer	PE		Human		National Institutes of Health, Bethesda, MD	31704 R
hMR1-6-FP tetramer	PE		Human		National Institutes of Health	31924 F

FITC, fluorescein isothiocyanate; PE, phycoerythrin.

cell subsets ($CD4^+$, $CD8^+$, and DN T cells) from each patient were randomly down-sampled to an equal number of events (5000 events). Flow cytometry data were transformed using an inverse hyperbolic sine function.

For identification of T-cell clusters, multiple runs of the DBSCAN were performed. For each cluster identified by DBSCAN, we quantified the differences between the frequency in HCC and nontumor liver samples and HCC and PBMC using the Wilcoxon signed-rank statistic test.

Figure 13. (***See previous page***). **Effect of nivolumab therapy on HCC patients.** (*A*, *E*, and *I*) tSNE maps of $CD8^+$ TILs from patients before nivolumab treatment. (*A* and *E*) Responder and (*I*) nonresponder patients. (*B*, *F*, and *J*) tSNE maps of $CD8^+$ TILs from patients on nivolumab therapy. (*B* and *F*) Responder and (*J*) nonresponder patients. (*C*, *G*, and *M*) tSNE maps indicating individual clusters of $CD8^+$ TILs in (*C* and *G*) responder and (*K*) nonresponder patients. (*D*, *H*, and *L*) Heatmaps of the normalized expression of each marker for indicated clusters. The *purple asterisks* indicate TIL clusters enriched in pretreatment samples and the *yellow asterisks* indicate TIL clusters enriched in on-therapy samples. Color scales indicate the relative expression levels of the indicated marker.

Statistical Analysis

The results are expressed as means ± SD. In all analyses, the Wilcoxon signed-rank test, adjusted with the Benjamini and Hochberg method and a 2-tailed paired test multicomparison (Tukey test) were used. A P value of .05 or less (95% CI) was considered statistically significant.

All authors had access to the study data and reviewed and approved the final manuscript.

References

1. Torre LA, Siegel RL, Ward EM, Jemal A. Global cancer incidence and mortality rates and trends–an update. Cancer Epidemiol Biomarkers Prev 2016;25:16–27.
2. Marquardt JU, Andersen JB, Thorgeirsson SS. Functional and genetic deconstruction of the cellular origin in liver cancer. Nat Rev Cancer 2015;15:653–667.
3. El-Serag HB. Hepatocellular carcinoma. N Engl J Med 2011;365:1118–1127.
4. Zamarron BF, Chen W. Dual roles of immune cells and their factors in cancer development and progression. Int J Biol Sci 2011;7:651–658.
5. Capece D, Fischietti M, Verzella D, Gaggiano A, Cicciarelli G, Tessitore A, Zazzeroni F, Alesse E. The inflammatory microenvironment in hepatocellular carcinoma: a pivotal role for tumor-associated macrophages. Biomed Res Int 2013;2013:187–204.
6. Chen DS, Mellman I. Elements of cancer immunity and the cancer-immune set point. Nature 2017;541:321–330.
7. Zheng X, Song X, Shao Y, Xu B, Chen L, Zhou Q, Hu W, Zhang D, Wu C, Tao M, Zhu Y, Jiang J. Prognostic role of tumor-infiltrating lymphocytes in gastric cancer: a meta-analysis. Oncotarget 2017;8:57386–57398.
8. Xu Q, Wang C, Yuan X, Feng Z, Han Z. Prognostic value of tumor-infiltrating lymphocytes for patients with head and neck squamous cell carcinoma. Transl Oncol 2017;10:10–16.
9. Foerster F, Hess M, Gerhold-Ay A, Marquardt JU, Becker D, Galle PR, Schuppan D, Binder H, Bockamp E. The immune contexture of hepatocellular carcinoma predicts clinical outcome. Sci Rep 2018;8:5351.
10. El-Khoueiry AB, Sangro B, Yau T, Crocenzi TS, Kudo M, Hsu C, Kim TY, Choo SP, Trojan J, Welling THR, Meyer T, Kang YK, Yeo W, Chopra A, Anderson J, Dela Cruz C, Lang L, Neely J, Tang H, Dastani HB, Melero I. Nivolumab in patients with advanced hepatocellular carcinoma (CheckMate 040): an open-label, non-comparative, phase 1/2 dose escalation and expansion trial. Lancet 2017;389:2492–2502.
11. Lepore M, Kalinichenko A, Colone A, Paleja B, Singhal A, Tschumi A, Lee B, Poidinger M, Zolezzi F, Quagliata L, Sander P, Newell E, Bertoletti A, Terracciano L, De Libero G, Mori L. Parallel T-cell cloning and deep sequencing of human MAIT cells reveal stable oligoclonal TCRbeta repertoire. Nat Commun 2014;5:3866.
12. Kurioka A, Walker LJ, Klenerman P, Willberg CB. MAIT cells: new guardians of the liver. Clin Transl Immunol 2016;5:e98.
13. Ye Q, Song DG, Poussin M, Yamamoto T, Best A, Li C, Coukos G, Powell DJ Jr. CD137 accurately identifies and enriches for naturally occurring tumor-reactive T cells in tumor. Clin Cancer Res 2014;20:44–55.
14. Hahsler MM. dbscan: density based clustering of applications with noise (DBSCAN) and related algorithms. R package version 1.0-0 2017. https://cran.r-project.org/web/packages/dbscan/vignettes/dbscan.pdf.
15. Chemnitz JM, Parry RV, Nichols KE, June CH, Riley JL. SHP-1 and SHP-2 associate with immunoreceptor tyrosine-based switch motif of programmed death 1 upon primary human T cell stimulation, but only receptor ligation prevents T cell activation. J Immunol 2004;173:945–954.
16. Petrovas C, Casazza JP, Brenchley JM, Price DA, Gostick E, Adams WC, Precopio ML, Schacker T, Roederer M, Douek DC, Koup RA. PD-1 is a regulator of virus-specific CD8+ T cell survival in HIV infection. J Exp Med 2006;203:2281–2292.
17. Kumar BV, Ma W, Miron M, Granot T, Guyer RS, Carpenter DJ, Senda T, Sun X, Ho SH, Lerner H, Friedman AL, Shen Y, Farber DL. Human tissue-resident memory T cells are defined by core transcriptional and functional signatures in lymphoid and mucosal sites. Cell Rep 2017;20:2921–2934.
18. Lukas Yani S, Keller M, Melzer FL, Weinberger B, Pangrazzi L, Sopper S, Trieb K, Lobina M, Orru V, Fiorillo E, Cucca F, Grubeck-Loebenstein B. CD8(+) HLADR(+) regulatory T cells change with aging: they increase in number, but lose checkpoint inhibitory molecules and suppressive function. Front Immunol 2018;9:1201.
19. Ganesan AP, Clarke J, Wood O, Garrido-Martin EM, Chee SJ, Mellows T, Samaniego-Castruita D, Singh D, Seumois G, Alzetani A, Woo E, Friedmann PS, King EV, Thomas GJ, Sanchez-Elsner T, Vijayanand P, Ottensmeier CH. Tissue-resident memory features are linked to the magnitude of cytotoxic T cell responses in human lung cancer. Nat Immunol 2017;18:940–950.
20. Park SL, Mackay LK, Gebhardt T. Distinct recirculation potential of CD69(+)CD103(-) and CD103(+) thymic memory CD8(+) T cells. Immunol Cell Biol 2016;94:975–980.
21. Kim R, Coppola D, Wang E, Chang YD, Kim Y, Anaya D, Kim DW. Prognostic value of CD8CD45RO tumor infiltrating lymphocytes in patients with extrahepatic cholangiocarcinoma. Oncotarget 2018;9:23366–23372.
22. Thommen DS, Koelzer VH, Herzig P, Roller A, Trefny M, Dimeloe S, Kiialainen A, Hanhart J, Schill C, Hess C, Savic Prince S, Wiese M, Lardinois D, Ho PC, Klein C, Karanikas V, Mertz KD, Schumacher TN, Zippelius A. A transcriptionally and functionally distinct PD-1(+) CD8(+) T cell pool with predictive potential in non-small-cell lung cancer treated with PD-1 blockade. Nat Med 2018;24:994–1004.
23. Wang X, Tian Z. Gammadelta T cells in liver diseases. Front Med 2018;12:262–268.
24. Hendry S, Salgado R, Gevaert T, Russell PA, John T, Thapa B, Christie M, van de Vijver K, Estrada MV, Gonzalez-Ericsson PI, Sanders M, Solomon B, Solinas C, Van den Eynden G, Allory Y, Preusser M, Hainfellner J,

Pruneri G, Vingiani A, Demaria S, Symmans F, Nuciforo P, Comerma L, Thompson EA, Lakhani S, Kim SR, Schnitt S, Colpaert C, Sotiriou C, Scherer SJ, Ignatiadis M, Badve S, Pierce RH, Viale G, Sirtaine N, Penault-Llorca F, Sugie T, Fineberg S, Paik S, Srinivasan A, Richardson A, Wang Y, Chmielik E, Brock J, Johnson DB, Balko J, Wienert S, Bossuyt V, Michiels S, Ternes N, Burchardi N, Luen SJ, Savas P, Klauschen F, Watson PH, Nelson BH, Criscitiello C, O'Toole S, Larsimont D, de Wind R, Curigliano G, Andre F, Lacroix-Triki M, van de Vijver M, Rojo F, Floris G, Bedri S, Sparano J, Rimm D, Nielsen T, Kos Z, Hewitt S, Singh B, Farshid G, Loibl S, Allison KH, Tung N, Adams S, Willard-Gallo K, Horlings HM, Gandhi L, Moreira A, Hirsch F, Dieci MV, Urbanowicz M, Brcic I, Korski K, Gaire F, Koeppen H, Lo A, Giltnane J, Rebelatto MC, Steele KE, Zha J, Emancipator K, Juco JW, Denkert C, Reis-Filho J, Loi S, Fox SB. Assessing tumor-infiltrating lymphocytes in solid tumors: a practical review for pathologists and proposal for a standardized method from the International Immuno-Oncology Biomarkers Working Group: part 2: TILs in melanoma, gastrointestinal tract carcinomas, non-small cell lung carcinoma and mesothelioma, endometrial and ovarian carcinomas, squamous cell carcinoma of the head and neck, genitourinary carcinomas, and primary brain tumors. Adv Anat Pathol 2017;24:311–335.

25. Denkert C, von Minckwitz G, Darb-Esfahani S, Lederer B, Heppner BI, Weber KE, Budczies J, Huober J, Klauschen F, Furlanetto J, Schmitt WD, Blohmer JU, Karn T, Pfitzner BM, Kummel S, Engels K, Schneeweiss A, Hartmann A, Noske A, Fasching PA, Jackisch C, van Mackelenbergh M, Sinn P, Schem C, Hanusch C, Untch M, Loibl S. Tumour-infiltrating lymphocytes and prognosis in different subtypes of breast cancer: a pooled analysis of 3771 patients treated with neoadjuvant therapy. Lancet Oncol 2018;19:40–50.
26. Lee N, Zakka LR, Mihm MC Jr, Schatton T. Tumour-infiltrating lymphocytes in melanoma prognosis and cancer immunotherapy. Pathology 2016;48:177–187.
27. Thommen DS, Schumacher TN. T cell dysfunction in cancer. Cancer Cell 2018;33:547–562.
28. Barnes TA, Amir E. HYPE or HOPE: the prognostic value of infiltrating immune cells in cancer. Br J Cancer 2018; 118:e5.
29. Pages F, Galon J, Dieu-Nosjean MC, Tartour E, Sautes-Fridman C, Fridman WH. Immune infiltration in human tumors: a prognostic factor that should not be ignored. Oncogene 2010;29:1093–1102.
30. Hwang WT, Adams SF, Tahirovic E, Hagemann IS, Coukos G. Prognostic significance of tumor-infiltrating T cells in ovarian cancer: a meta-analysis. Gynecol Oncol 2012;124:192–198.
31. Adams S, Gray RJ, Demaria S, Goldstein L, Perez EA, Shulman LN, Martino S, Wang M, Jones VE, Saphner TJ, Wolff AC, Wood WC, Davidson NE, Sledge GW, Sparano JA, Badve SS. Prognostic value of tumor-infiltrating lymphocytes in triple-negative breast cancers from two phase III randomized adjuvant breast cancer trials: ECOG 2197 and ECOG 1199. J Clin Oncol 2014; 32:2959–2966.
32. Lu L, Bai Y, Wang Z. Elevated T cell activation score is associated with improved survival of breast cancer. Breast Cancer Res Treat 2017;164:689–696.
33. Zheng C, Zheng L, Yoo JK, Guo H, Zhang Y, Guo X, Kang B, Hu R, Huang JY, Zhang Q, Liu Z, Dong M, Hu X, Ouyang W, Peng J, Zhang Z. Landscape of infiltrating T cells in liver cancer revealed by single-cell sequencing. Cell 2017;169:1342–1356 e1316.
34. Inada Y, Mizukoshi E, Seike T, Tamai T, Iida N, Kitahara M, Yamashita T, Arai K, Terashima T, Fushimi K, Yamashita T, Honda M, Kaneko S. Characteristics of immune response to tumor-associated antigens and immune cell profile in patients with hepatocellular carcinoma. Hepatology 2019;69:653–665.
35. Ou X, Guan J, Chen JS, Ying JC, Liu XP, Tian PK, Liu JK, Nie LP, Zhao Y, Yu GY. LAP(+)CD4(+) T cells are elevated among the peripheral blood mononuclear cells and tumor tissue of patients with hepatocellular carcinoma. Exp Ther Med 2018;16:788–796.
36. Lim CJ, Lee YH, Pan L, Lai L, Chua C, Wasser M, Lim TKH, Yeong J, Toh HC, Lee SY, Chan CY, Goh BK, Chung A, Heikenwalder M, Ng IO, Chow P, Albani S, Chew V. Multidimensional analyses reveal distinct immune microenvironment in hepatitis B virus-related hepatocellular carcinoma. Gut 2019;68:916–927.
37. Osorio JC, Harding JJ. Understanding and quantifying the immune microenvironment in hepatocellular carcinoma. Transl Gastroenterol Hepatol 2018;3:107.
38. Wolfl M, Kuball J, Ho WY, Nguyen H, Manley TJ, Bleakley M, Greenberg PD. Activation-induced expression of CD137 permits detection, isolation, and expansion of the full repertoire of CD8+ T cells responding to antigen without requiring knowledge of epitope specificities. Blood 2007;110:201–210.
39. Simpson TR, Quezada SA, Allison JP. Regulation of CD4 T cell activation and effector function by inducible costimulator (ICOS). Curr Opin Immunol 2010; 22:326–332.
40. Zhu Y, Chen L. CD137 as a biomarker for tumor-reactive T cells: finding gold in the desert. Clin Cancer Res 2014; 20:3–5.
41. Pauken KE, Wherry EJ. TIGIT and CD226: tipping the balance between costimulatory and coinhibitory molecules to augment the cancer immunotherapy toolkit. Cancer Cell 2014;26:785–787.
42. Wherry EJ. T cell exhaustion. Nat Immunol 2011; 12:492–499.
43. Tu JF, Ding YH, Ying XH, Wu FZ, Zhou XM, Zhang DK, Zou H, Ji JS. Regulatory T cells, especially ICOS(+) FOXP3(+) regulatory T cells, are increased in the hepatocellular carcinoma microenvironment and predict reduced survival. Sci Rep 2016;6:35056.
44. De Simone M, Arrigoni A, Rossetti G, Gruarin P, Ranzani V, Politano C, Bonnal RJP, Provasi E, Sarnicola ML, Panzeri I, Moro M, Crosti M, Mazzara S, Vaira V, Bosari S, Palleschi A, Santambrogio L, Bovo G, Zucchini N, Totis M, Gianotti L, Cesana G, Perego RA, Maroni N, Pisani Ceretti A, Opocher E, De Francesco R, Geginat J, Stunnenberg HG, Abrignani S, Pagani M. Transcriptional landscape of human tissue lymphocytes

unveils uniqueness of tumor-infiltrating T regulatory cells. Immunity 2016;45:1135–1147.
45. Plitas G, Konopacki C, Wu K, Bos PD, Morrow M, Putintseva EV, Chudakov DM, Rudensky AY. Regulatory T cells exhibit distinct features in human breast cancer. Immunity 2016;45:1122–1134.
46. Tanchot C, Terme M, Pere H, Tran T, Benhamouda N, Strioga M, Banissi C, Galluzzi L, Kroemer G, Tartour E. Tumor-infiltrating regulatory T cells: phenotype, role, mechanism of expansion in situ and clinical significance. Cancer Microenviron 2013;6:147–157.
47. Gao B, Jeong WI, Tian Z. Liver: An organ with predominant innate immunity. Hepatology 2008;47:729–736.
48. Mehal WZ, Azzaroli F, Crispe IN. Immunology of the healthy liver: old questions and new insights. Gastroenterology 2001;120:250–260.
49. Mori L, Lepore M, De Libero G. The Immunology of CD1- and MR1-restricted T cells. Annu Rev Immunol 2016; 34:479–510.
50. Godfrey DI, Le Nours J, Andrews DM, Uldrich AP, Rossjohn J. Unconventional T cell targets for cancer immunotherapy. Immunity 2018;48:453–473.
51. Silva-Santos B, Serre K, Norell H. Gammadelta T cells in cancer. Nat Rev Immunol 2015;15:683–691.
52. Ma CS, Nichols KE, Tangye SG. Regulation of cellular and humoral immune responses by the SLAM and SAP families of molecules. Annu Rev Immunol 2007; 25:337–379.
53. Ayers M, Lunceford J, Nebozhyn M, Murphy E, Loboda A, Kaufman DR, Albright A, Cheng JD, Kang SP, Shankaran V, Piha-Paul SA, Yearley J, Seiwert TY, Ribas A, McClanahan TK. IFN-gamma-related mRNA profile predicts clinical response to PD-1 blockade. J Clin Invest 2017;127:2930–2940.
54. Patel SJ, Sanjana NE, Kishton RJ, Eidizadeh A, Vodnala SK, Cam M, Gartner JJ, Jia L, Steinberg SM, Yamamoto TN, Merchant AS, Mehta GU, Chichura A, Shalem O, Tran E, Eil R, Sukumar M, Guijarro EP, Day CP, Robbins P, Feldman S, Merlino G, Zhang F, Restifo NP. Identification of essential genes for cancer immunotherapy. Nature 2017;548:537–542.
55. Edmondson HA, Steiner PE. Primary carcinoma of the liver: a study of 100 cases among 48,900 necropsies. Cancer 1954;7:462–503.
56. van der Maaten L. Accelerating t-SNE using tree-based algorithms. J Machine Learning Res 2014; 15:3221–3245.

Received February 26, 2019. Accepted August 9, 2019.

Correspondence
Address correspondence to: Gennaro De Libero, MD, or Markus H. Heim, MD, Department of Biomedicine, University of Basel, Hebelstrasse 20, 4031 Basel, Switzerland. e-mail: markus.heim@unibas.ch or gennaro.delibero@unibas.ch; fax: +41 61 265 23 50.

Acknowledgments
The authors thank Tobias Rutishauser for help in setting a computational analysis pipeline and P. Cullen for revising the manuscript. The MR1 tetramer technology was developed jointly by Dr James McCluskey, Dr Jamie Rossjohn, and Dr David Fairlie, and the material was produced by the National Institutes of Health Tetramer Core Facility as permitted to be distributed by the University of Melbourne.

Author contributions
Daniela Di Blasi designed and performed experiments, analyzed data, and wrote the manuscript; Tujana Boldanova and Markus H. Heim recruited patients, performed biopsies, and collected and curated clinical annotation data; Luigi Terracciano performed the histopathologic analysis; Lucia Mori discussed the data and wrote the manuscript; Markus H. Heim and Gennaro De Libero conceived and designed experiments, coordinated the study, supervised the work and the interpretation of the results, and obtained funding; and Gennaro De Libero wrote the manuscript.

Conflicts of interest
The authors disclose no conflicts.

Funding
This work was supported by grants SNF 310030-173240, KFS-3730-08-2015, and PMB-02-17 (G.D.L.), and by European Research Council Synergy 609883 Mechanisms of Evasive Resistance in Cancer (MERiC) and SystemX (MERIC) (M.H.H.).